Computational Materials Science 63 (2012) 75–90

Contents lists available at SciVerse ScienceDirect

Computational Materials Science

journal homepage: www.elsevier.com/locate/commatsci

Computer simulations of electrodiffusion problems based on Nernst–Planck and Poisson equations

J.J. Jasielec [a], R. Filipek [b,*], K. Szyszkiewicz [b,c], J. Fausek [b], M. Danielewski [b], A. Lewenstam [a,b]

[a] Process Chemistry Centre, c/o Centre for Process Analytical Chemistry and Sensor Technology (ProSens), Åbo Akademi University, Biskopsgatan 8, 20500 Åbo-Turku, Finland
[b] The Faculty of Materials Science and Ceramics, Interdisciplinary Centre of Materials Modelling, AGH University of Science and Technology, Al. Mickiewicza 30, 30-059 Kraków, Poland
[c] The Faculty of Computer Sciences, WSB-NLU, Zielona 27, 33-300 Nowy Sącz, Poland

ARTICLE INFO

Article history:
Received 18 February 2012
Received in revised form 16 May 2012
Accepted 21 May 2012
Available online 29 June 2012

Keywords:
Electrodiffusion
Ion transport
Nernst–Planck–Poisson
Neumann and Dirichlet boundary conditions
Method of lines
Consistency
Liquid junction
Binary electrolyte
Bi-ionic case
Ion selective electrodes
Sensors
Electrochemical impedance spectroscopy

ABSTRACT

A numerical procedure based on the method of lines for time-dependent electrodiffusion transport has been developed. Two types of boundary conditions (Neumann and Dirichlet) are considered. Finite difference space discretization with suitably selected weights based on a non-uniform grid is applied. Consistency of this method and the method put forward by Brumleve and Buck are analysed and compared. The resulting stiff system of ordinary differential equations is effectively solved using the RADAU5, RODAS and SEULEX integrators. The applications to selected electrochemical systems: liquid junction, bi-ionic case, ion selective electrodes and electrochemical impedance spectroscopy have been demonstrated. In the paper we promote the use of the full form of the Nernst–Planck and Poisson (NPP) equations, that is including explicitly the electric field as an unknown variable with no simplifications like electroneutrality or constant field assumptions. An effective method of the numerical solution of the NPP problem for arbitrary number of ionic species and valence numbers either for a steady state or a transient state is shown. The presented formulae – numerical solutions to the NPP problem – are ready to be implemented by anyone. Moreover, we make the resulting software freely available to anybody interested in using it.

1. Introduction

Mass and charge transport processes play an important role in different areas of science. In electrochemistry they are extensively used for the description of membrane potentials and concentration profiles. Particular application of this description is the field of ion selective electrodes (ISEs) and molten salts. In engineering problems the behaviour of porous materials is affected by the transport of ions due to concentration gradients. These mechanisms of ionic diffusion in porous media which appear, for example in the filtration by ion exchange membranes and the transport of pollutants in soils, have received a great deal of attention from chemical and geological engineers. The process of ionic diffusion remains of primary importance in many civil engineering problems since the long-term durability of many building materials, such as concrete, is directly effected by the transport of chemical species [1]. In semiconductor field the transport of charged species was considered from the very beginnings of this discipline. Workers in this field developed many powerful techniques but usually directed to solve its specific problems (two species and steady-state). The membrane processes involving charge transport are also of vital importance in cell biology since they support homeostasis of living organisms.

All these processes (ionic diffusion in porous media, electrochemical and biological membranes as well as electrons and holes transport in semiconductors) can be described using Nernst–Planck and Poisson (NPP) system of partial differential equations with suitable initial and boundary conditions. Although, tools for modelling individual applications are described in literature yet, they are not easy to get. Some of them are commercial (e.g., COMSOL), some use commercial computation environments (e.g., Mathematica, Mathcad, MATLAB), and others require to buy the commercial specialised numerical libraries (like DiffPack, NAG, IMSL, etc.).

In this paper we will promote the use of full form of NPP equations, i.e., including explicitly the electric field as an unknown variable. We will present an effective method of numerical solution of NPP problem for arbitrary number of ionic species and valence numbers, both for steady and transient states. A new discretization

* Corresponding author. Tel.: +48 12 617 32 31; fax: +48 12 617 24 93.
E-mail address: rof@agh.edu.pl (R. Filipek).

0927-0256/$ - see front matter © 2012 Elsevier B.V. All rights reserved.
http://dx.doi.org/10.1016/j.commatsci.2012.05.054

scheme is presented and its consistency is analysed. Two types of boundary conditions are considered: (1) Neumann-like boundary conditions for fluxes–known in electrochemistry as Chang–Jaffé boundary conditions and (2) Dirichlet boundary condition for concentrations. Obtained formulae – expressions for numerical solution to NPP problem – can be used by anyone interested to implement them on their own. Moreover we make the resulting software available to anybody interested in using it.

The plan of this paper is as follows. We start from the short introduction to NPP equations with Dirichlet and Neumann-like boundary conditions. A method of lines using new space discretization scheme is described and used for obtaining numerical solution of initial-boundary value problem for the NPP system. This method is tested for a binary electrolyte case, where an analytical solution for transient state is available. The use of the software for solving liquid junction and bi-ionic cases is also demonstrated. Application to ion-selective electrodes are shown and compared with experimental results. Generation of impedance spectra based on the time dependent solution of NPP problem is also presented.

2. Mathematical model

The multi-layer NPP model describes a system consisting of α layers, each corresponding to a different phase Fig. 1. This transient model of electrodiffusion allows a description of the evolution of ionic concentrations and electric potential profiles in time, and is often used in modelling of transport in liquid and solid electrolytes, melted salts, oxide scales, etc. In this model, diffusion and migration of ions are governed according to the Nernst–Planck (NP) flux expression, while the Poisson (P) equation describes the electrical interaction of the species. However, it is convenient to replace the Poisson equation by the displacement current equation as described by Cohen and Cooley [2]. All these equations form the following system of evolutionary nonlinear partial differential equations (PDEs) for r components and α layers:

$$\begin{cases} \frac{\partial c_i^j}{\partial t}(x,t) = -\frac{\partial J_i^j}{\partial x}(x,t) \quad \text{for} \quad i = 1,\dots,r, \\ \frac{\partial E^j}{\partial t}(x,t) = \frac{1}{\varepsilon_j} I(t) - \frac{F}{\varepsilon_j}\sum_{i=1}^{r} z_i J_i^j(x,t), \\ x \in [\lambda_{j-1},\lambda_j] \text{ for each layer } j = 1,\dots,\alpha, \\ t \in [0, t_{END}], \end{cases} \tag{1}$$

where the expression for the Nernst–Planck flux (*constitutive relation*) is

$$J_i^j(x,t) = -D_i^j \frac{\partial c_i^j}{\partial x}(x,t) + \frac{F}{RT} D_i^j z_i \left(c_i^j E^j\right)(x,t). \tag{2}$$

In the above equations c_i^j – the molar concentration of i-th component in j-th layer, E^j – the electric field in j-th layer, $I(t)$ – the electrical current density, ε_j – dielectric constant of j-th layer, λ_{j-1},λ_j – the boundaries of j-th layer, z_i – the valence number of i-th component, t_{END} – duration of the process, and F, R, T have their usual meanings (the Faraday constant, gas constant and absolute temperature).

For completeness, the above system of PDE must be accompanied by boundary and initial conditions. The initial conditions consist of given concentration profiles and electric field:

$$c_i^j(x,0) = c_{0,i}^j(x), \quad E^j(x,0) = E_0(x), \ \text{for } x \in [\lambda_{j-1},\lambda_j], \quad i = 1,\dots,r, \quad j = 1,\dots,\alpha. \tag{3}$$

$E_0(x)$ is assumed to be zero for all x except in the case of impedance spectra simulations. In simulations we used electroneutral initial profiles, although it is not necessary.

The boundary conditions may be of various types. In this paper we use two types of boundary conditions. The first are the Neumann-like boundary conditions for fluxes [3], known in electrochemistry as Chang–Jaffé boundary conditions. The first order heterogeneous rate constants $\vec{k}_i^j, \overleftarrow{k}_i^j$ are used to describe the kinetics at the interface $x = \lambda_j$ between the layers j and $j+1$:

$$J_i^j(\lambda_j,t) = J_i^{j+1}(\lambda_j,t) = \vec{k}_i^j c_i^j(\lambda_j,t) - \overleftarrow{k}_i^j c_i^{j+1}(\lambda_j,t). \tag{4}$$

The above equation is a special case of Butler–Volmer equation, when the overpotential equals zero [4].

The second possibility (basically for single-layer problems, $\alpha = 1$) is the standard Dirichlet boundary conditions for concentrations

$$\begin{aligned} &c_i^1(\lambda_0,t) = c_{i,L} = const, \\ &c_i^1(\lambda_1,t) = c_{i,R} = const \ \text{for} \ \ i = 1,\dots,r, \end{aligned} \tag{5}$$

where $c_{i,L}, c_{i,R}$ are the left and right bulk concentrations [5,6]. The use of both types of boundary conditions will be presented for liquid junction case.

Scaling and dimensionless variables The presented problem contains many physical parameters. By introducing dimensionless variables, the number of these parameters can be reduced. Moreover, by finding the proper scaling factors it is possible to identify the relative contribution of the various terms in the equations. This may be used to obtain better accuracy in numerical procedures. Thus, the Eqs. (1)–(5) may now be converted into a dimensionless form [7] through the following transformations:

$$\begin{aligned} &\bar{x} := x/x_s, \quad \bar{t} := t/t_s, \quad \bar{c}_i^j(\bar{x},\bar{t}) := c_i^j(x_s\bar{x}, t_s\bar{t})/c_s, \\ &\bar{E}^j(\bar{x},\bar{t}) := E^j(x_s\bar{x}, t_s\bar{t})/E_s, \end{aligned} \tag{6}$$

where x, t, c_i^j, E^j and $\bar{x}, \bar{t}, \bar{c}_i^j, \bar{E}_i^j$ are physical and dimensionless values of distance, time, concentration and electric field respectively; x_s, t_s, c_s, E_s are their characteristic values (scaling factors). Dimensionless parameters take the form: $\bar{D}_i^j = \frac{t_s}{x_s^2} D_i^j$, $\bar{\vec{k}}_i^j = \frac{t_s}{x_s}\vec{k}_i^j$, $\bar{\overleftarrow{k}}_i^j = \frac{t_s}{x_s}\overleftarrow{k}_i^j$, $\bar{\lambda}_j = \lambda_j/x_s$.

From this point on, we use the rescaled variables in all equations and the overbars are dropped to ease the burden of notation.

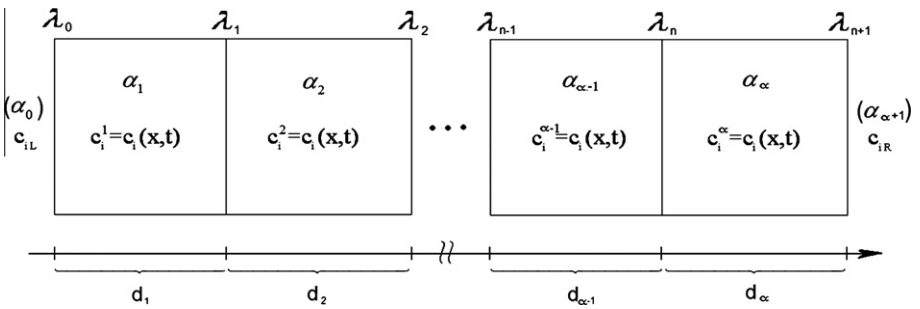

Fig. 1. Schematic representation of the system for NPP model of electrodiffusion.

The following set of equations express the dimensionless model of electrodiffusion:

$$\begin{cases} \frac{\partial c_i^j}{\partial t} = -\frac{\partial J_i^j}{\partial x}, \\ \frac{\partial E^j}{\partial t} = I(t) - \Lambda_j \sum_{i=1}^{r} z_i J_i^j \quad \text{for } j = 1,\ldots,\alpha, \quad i = 1,\ldots,r, \end{cases} \tag{7}$$

where the rescaled flux is given as $J_i^j = -D_i^j\left(\partial c_i^j/\partial x\right) + z_i D_i^j c_i^j E^j$, D_i^j – rescaled diffusion coefficient, Λ_j is defined by: $\Lambda_j = c_s x_s F/(E_s \varepsilon_j)$, $E_s = RT/(Fx_s)$ and F, R, T, ε_j have their usual meaning.

Rescaled initial and boundary conditions take the form given by Eqs. (3)–(5).

2.1. Numerical method

Some numerical treatments of the Nernst–Planck and Poisson equations (NPP) lead to the problem of solving a system of ordinary differential equations (ODEs) $\frac{dy}{dt} = f(t,y)$, where $f : \mathbb{R}^n \to \mathbb{R}^n$, $y = y(t) \in \mathbb{R}^n$. The numerical procedures for ODEs can be broadly divided into two categories: *explicit* and *implicit* [7–9]. In explicit methods the passage from time t_k to $t_{k+1} = t_k + \Delta t$ is carried out simply by one-step evaluation of expression which is defined by the method. This can be exemplified by the explicit Euler method where advancement $t_k \to t_{k+1}$ is performed as follows: $y_{k+1} = y_k + \Delta t \cdot f(t_k, y_k)$. We see that this is just equivalent to evaluation of $f(t,y)$ for $t = t_k$ and $y = y_k$. On the other hand, in the implicit methods, obtaining the approximation of the solution for $t_{k+1} = t_k + \Delta t$ requires solving a system of (usually) nonlinear equations. For example, to obtain y_{k+1} in the implicit Euler method, the following equation: $y_{k+1} = y_k + \Delta t \cdot f(t_{k+1}, y_{k+1})$ must be solved with respect to y_{k+1}.

In 1965 Cohen and Cooley [2] were the first who developed a numerical procedure for the time dependent NPP using *explicit* method. In 1975 Sandifer and Buck [10] introduced a mixed implicit (for electric field) and explicit (for concentration) method similar to that of Cohen and Cooley [2]. However, due to explicit nature of concentration calculation their method suffered from very small time step of integration and consequently was time-consuming. The same equations as NPP are used to describe transport processes in semiconductor devices. Of particular interest in that area is the procedure put forward by Scharfetter and Gummel [11]. These authors used an improved flux equation obtained by integration with respect to the concentration of the Nernst–Planck equation while holding the flux and electric field constant in each volume element. The time step integration was performed using Crank–Nicolson method [12]. A substantial contribution to numerical treatment of NPP with applications to membrane electrochemistry is a seminal paper by Brumleve and Buck (1977) [5]. These authors developed an efficient finite difference simulation procedure for multi-component NPP equations using fully implicit time scheme that was subsequently solved by the Newton–Raphson technique [8]. Their approach has been used by many authors since [6,13–15]. However the question of convergence of Brumleve and Buck method was not analysed. As the authors wrote "*(...) derivation of the truncation error for the complete non-linear system is beyond the scope of this treatment*". It means that the authors assumed the procedure is consistent and the simulations they performed just confirm that assumption. In this paper a new discretization scheme is presented, its consistency is analysed and compared to that of Brumleve and Buck.

The method of lines [16] will be employed to solve numerically the ODEs system resulting from the space discretization of the NPP equations. Generally, non-uniform grids are used. This allows a better approximations in areas where larger gradients of profiles are expected. For example in a typical ISE modelling a denser grid near boundaries is used – see details in Appendix B. The grid non-uniformity requires the use of finite differences with properly selected weights [7], Chap. 3, [17,18]. The concentrations are defined at points $y_{j,k}$ while the electric field and fluxes at points $x_{j,k}$ (Fig. 2). Each point $y_{j,k}$ is placed in the middle of the interval $[x_{j,k-1}, x_{j,k}]$, hence $y_{j,k} = \frac{1}{2}(x_{j,k-1} + x_{j,k})$. Some authors use different notations, namely $x_{j,k\pm1/2} = \frac{1}{2}(x_{j,k\pm1} + x_{j,k})$.

The finite difference approximation of continuity equation which corresponds to the above grid for internal nodes reads

$$\begin{aligned} \frac{dc_i^{j,k}}{dt}(t) &:= \frac{\partial c_i^j}{\partial t}(y_{j,k},t) = -\frac{\partial J_i^j}{\partial x}(y_{j,k},t) \approx -\frac{J_i^j(x_{j,k},t) - J_i^j(x_{j,k-1},t)}{h_{k-1}}, \\ J_i^{j,k}(t) &= J_i^j(x_{j,k},t) = -D_i^j\left(\frac{\partial c_i^j}{\partial x}(x_{j,k},t) - z_i c_i^j(x_{j,k},t)E^j(x_{j,k},t)\right) \\ &\approx -D_i^j\left(2\frac{h_{j,k-1}^2 c_i^{j,k+1} - h_{j,k}^2 c_i^{j,k} + (h_{j,k}^2 - h_{j,k-1}^2)c_i^{j,k}}{h_{j,k-1}h_{j,k}(h_{j,k-1}+h_{j,k})} - z_i c_i^j(x_{j,k},t)E^{j,k}\right) \\ &\approx -D_i^j\left(2\frac{h_{j,k-1}^2 c_i^{j,k+1} - h_{j,k}^2 c_i^{j,k} + (h_{j,k}-h_{j,k-1})(h_{j,k}c_i^{j,k} + h_{j,k-1}c_i^{j,k+1})}{h_{j,k-1}h_{j,k}(h_{j,k-1}+h_{j,k})}\right. \\ &\left. - z_i\frac{h_{j,k}c_i^{j,k} + h_{j,k-1}c_i^{j,k+1}}{h_{j,k-1}+h_{j,k}}E^{j,k}\right) \text{ for } i = 1,\ldots,r, \quad j = 1,\ldots,\alpha \text{ and} \\ &k = 1,\ldots, \quad N_j - 1. \end{aligned} \tag{8}$$

and for boundary nodes the one-sided non-uniform finite differences (Appendix A) are used

$$\begin{aligned} \frac{dc_i^{j,0}}{dt} &= \frac{-h_{j,1}(2h_{j,0}+h_{j,1})J_i^{j,0} + (h_{j,0}+h_{j,1})^2 J_i^{j,1} - h_{j,0}^2 J_i^{j,2}}{h_{j,0}h_{j,1}(h_{j,0}+h_{j,1})}, \quad \frac{dc_i^{j,N+1}}{dt} \\ &= \frac{h_{j,N-1}^2 J_i^{j,N-2} - (h_{j,N-1}+h_{j,N-2})^2 J_i^{j,N-1} + h_{j,N-2}(h_{j,N-2}+2h_{j,N-1})J_i^{j,N}}{h_{j,N-1}h_{j,N-2}(h_{j,N-2}+h_{j,N-1})}, \end{aligned} \tag{9}$$

where $c_i^{j,k} = c_i^j(y_{j,k},t), E^{j,k} = E^j(x_{j,k},t)$ and $J_i^{j,k} = J_i^j(x_{j,k},t)$. The space derivative of the concentration at $x_{j,k}$ was approximated by a three-point non-uniform finite difference (Appendix A) and the concentration at $x_{j,k}$ by a weighted linear combination of the neighbouring concentrations as follows $c_i^j(x_k,t) \approx \left(h_{j,k}c_i^{j,k} + h_{j,k-1}c_i^{j,k+1}\right)/(h_{j,k-1}+h_{j,k})$ (Fig. 2). This type of discretization ensures that space local truncation error is of second order (*cf.* Britz 7, Sec. 3.8).

The finite difference approximation of displacement current equation corresponding to the grid (Fig. 2) reads

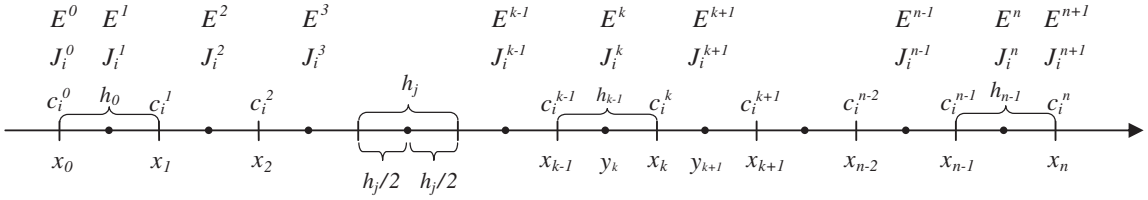

Fig. 2. Space grid for electrodiffusion problem, where $J_i^{j,k}(t) = J_i(x_{j,k},t), c_i^{j,k}(t) = c_i(y_{j,k},t), j = 1,\ldots,\alpha$ and $i = 1,\ldots,r$.

$$\frac{dE^{j,k}}{dt} = I(t) - \Lambda_j \sum_{i=1}^{r} z_i J_i^{j,k} \text{ for } k = 0, \ldots, N_j. \tag{10}$$

Case 1: Neumann-like boundary conditions

The flux at the boundary is given by the Chang–Jaffé formula

$$J_i^{j,N} = J_i^{j+1,0} = \vec{k}_i^j c_i^{j,N} - \overleftarrow{k}_i^j c_i^{j+1,0}(\lambda_j, t). \tag{11}$$

The Chang–Jaffé boundary conditions are the special case of Butler–Volmer boundary conditions with zero overpotential.

Case 2: Dirichlet boundary conditions

These conditions considers constant concentrations at the boundaries, therefore can be used for one layer system only, otherwise we would obtain independent system for each layer. In order to ease the burden of notation, from now on and for all cases where only one layer is considered, index $j = 1$ is omitted (e.g. $c_i^k = c_i^{1,k}, h_k = h_{1,k}$). For boundary nodes concentrations are given

$$c_i^0 = c_{i,L}, \quad c_i^N = c_{i,R} \text{ for } i = 1, \ldots, r \tag{12}$$

and the fluxes at the boundary are discretized as follows

$$J_i^0 \approx -D_i \left(2\frac{-(h_0+h_1)(3h_0+h_1)c_{i,L} + (2h_0+h_1)^2 c_i^1 + h_0^2 c_i^2}{h_0(h_0+h_1)(2h_0+h_1)} - z_i c_{i,L} E^0 \right),$$
$$J_i^N \approx -D_i \left(2\frac{h_{N-1}^2 c_i^{N-2} - (2h_{N-1}+h_{N-2})^2 c_i^{N-1} + (h_{N-2}+h_{N-1})(h_{N-2}+3h_{N-1})c_{i,R}}{h_{N-1}(h_{N-2}+h_{N-1})(h_{N-2}+2h_{N-1})} - z_i c_{i,R} E^N \right). \tag{13}$$

The above discretization leads to the system of ordinary differential equations (ODEs) in time variable. Due to *stiffness* nature of this ODEs special integrators are needed (e.g., RADAU5 (Radau IIA) [19], Gear [20], Rosenbrock [21]).

2.2. Local truncation error

A fundamental issue of any numerical procedure is the question of convergence. While we cannot claim that convergence was proved here it is expected that one of the factors that may have impact on the quality of such procedure is the order of local truncation error (LTE). This is due to the fact that for the finite difference approximation of the linear parabolic PDEs one can use the fundamental Lax theorem [22], which states that for such equations the convergence of the discretisation scheme is equivalent to its consistency and stability. The NPP system is of course nonlinear, hence this theorem does not apply to it. Nevertheless it is reasonable to assume that the higher the order of LTE the better convergence is to be expected. The local truncation error LTE is a grid function defined as follows: if (c, E) is the true solution of the NPP problem (7), then we can calculate the value of the finite difference expression (e.g. (8)) after substituting into it the values taken from this true solution (i.e. $c_i^{j,k}(t) = c_i^j(y_k, t)$ and so on). Now the LTE defined as the difference between such calculated value and the value of the right-hand side of the Eq. (7) evaluated using (c, E) (the true solution). In other words the LTE measures the error introduced by the evaluating the finite difference expression instead of evaluating the right-hand side of the equations (which contains derivatives). Derivation of the LTE both for Brumleve–Buck [5] and our approach was carried out revealing the following estimates.

$$\begin{aligned} &\textit{Brumleve Buck}: \quad LTE = O\left(\frac{2(h_{j,k-1}+h_{j,k})}{h_{j,k-2}+2h_{j,k-1}+h_{j,k}} - 1\right) + O(\delta), \\ &\textit{Our method}: \quad LTE = O(h_{j,k} - h_{j,k-1}) + O(\delta^2), \end{aligned} \tag{14}$$

where $\delta = \max\{h_{j,k}\}$. Thus, for our method $\lim_{\delta \to 0} LTE = 0$, which means consistency. In the case of Brumleve–Buck $\lim_{\delta \to 0} LTE = 0$ but only if additional conditions are imposed (e.g., $h_{j,k}/h_{j,k-1} \to 1$). Moreover the LTE approximation is one order higher for our method. (Notation $g(x) = O(f(x))$ means that there exists $M > 0$ such that $|g(x)| \leqslant M \cdot f(x)$).

2.3. Computer implementations

Discretization formulae shown in (8)–(13) are sufficiently detailed to allow anyone interested to implement the computations. However, due to the *stiffness* nature of this ODEs a special integrator is needed. The source of the stiffness is connected with the method of lines which tends to produce this phenomena for diffusion terms [23]. In this paper three different integrators have been used: RADAU5 [9], RODAS [21], and SOULEX [9]. The first two are based on the special types of *implicit* Runge–Kutta methods and the third is based on the extrapolation applied to *linearly implicit* Euler method.

Their time performance for typical electrodiffusion problems has been presented in [24]. It can be noted that none of them is suitable for all cases. For the cases of ISE and bi-ionic systems the best performance was exhibited by the SEULEX solver, while for the liquid junction it was the RODAS solver. Comparisons of the integrators' performance show that in many cases the most efficient one is the SEULEX algorithm. However, the performance may strongly depend on the specific values of physical parameters, e.g. boundary concentrations or heterogeneous rate constants.

Following our idea of taking into account the electric field in electrochemical simulations we make a C++ implementation available free of charge for anyone interested in this field. For a single-layer system a computer software (including full source code) being a part of CADA environment (Computer Aided Diffusion Analysis) may be downloaded from http://www.cada.agh.edu.pl

3. Applications

In this section the presented method of the numerical solution to the NPP problem is tested for various cases: liquid junction, bi-ionic case, and ion selective electrode. Two types of boundary conditions are used: Dirichlet and Neumann-like. The results of calculation obtained from our method are compared with an analytical solution, the results of other authors (different methods), and with experimental data.

3.1. Liquid junction potential

The numerical method was tested for historically important results, that is the junction potentials formed over a "*watery contact zone*". The concept of the liquid junction was developed by Nernst [25] and Planck [26]. Recent review of work concerned with analysis and simulation of liquid junction potentials can be found in [27].

A watery contact zone may be described as an imaginary barrier, of limited width, separating two different bathing solutions possessing the same physical characteristics as water. This approach, used by Planck [26,28], has been widely used ever since. Dickinson et al. [27] in their recent work presented alternative

approach. Instead of the unphysical barrier [15], they used a dynamically moving junction of two liquids in linear semi-infinite space.

In this paper, the steady state values obtained by our method at "infinite time" are compared with the published values according to Planck, Henderson, and the evolutional method described by Sokalski and Lewenstam [29].

Planck method [26,28]. Planck considered single charged ions, $z_i = \pm 1$ and assumed electroneutrality, $\sum_i c_i^+(x) = \sum_i c_i^-(x)$ for $0 \leqslant x \leqslant d$. Using the Dirichlet boundary conditions, $c_i(0) = c_{i,L}, c_i(d) = c_{i,R}$, he derived the formula for a steady-state diffusion potential[1]:

$$\Phi = \frac{RT}{F} \ln \xi, \tag{15}$$

where ξ is a solution of the following non-linear transcendental equation:

$$\frac{\xi u_R^+ - u_L^+}{u_R^- - \xi u_L^-} = \frac{\ln c - \ln \xi}{\ln c + \ln \xi} \frac{\xi c - 1}{c - \xi}, \tag{16}$$

with $u_L^+ = \sum_i c_{i,L}^+ D_i^+, u_L^- = \sum_i c_{i,L}^- D_i^-, u_R^+ = \sum_i c_{i,R}^+ D_i^+, u_R^- = \sum_i c_{i,R}^- D_i^-, c_L = \sum_{i=1}^r c_{i,L}, c_R = \sum_{i=1}^r c_{i,R}, c = c_R/c_L$.

The Henderson method [30,31] gives an expression for a membrane potential [4], based on the assumption that concentrations at a steady state in the membrane are linear in space

$$c_i(x) = c_i(0) + (c_i(d) - c_i(0))x/d, \tag{17}$$

and that the electric current is null ("zero-current") at such state: $\sum_i z_i J_i = 0$. This equation combined with (2) and (17) gives the well-known formula:

$$\Phi = -\int_0^d E(x)dx = -\frac{RT}{F} \frac{\sum_{i=1}^r z_i D_i (c_i(d) - c_i(0))}{\sum_{i=1}^r z_i^2 D_i (c_i(d) - c_i(0))} \ln \left(\frac{\sum_{i=1}^r z_i^2 D_i c_i(d)}{\sum_{i=1}^r z_i^2 D_i c_i(0)} \right). \tag{18}$$

The Planck equation reduces to the form equivalent to the Henderson equation in two following cases: (1) a junction of two A^+ X^- solutions of different concentrations and (2) a junction of two solutions A^+ X^- and B^+ X^- with common concentration. This corresponds to liquid junction type 1 and 2 in Lingane's classification [32].

The Sokalski–Lewenstam method [6,29]. Liquid junction potential is calculated as an asymptotic steady-state solution of the time-dependent NPP problem assuming "infinite" heterogeneous rate constants. They used an implicit Euler time discretization scheme and conditionally consistent space discretization (first applied by Brumleve and Buck [5]). In this method an arbitrary time step is chosen. The resulting system of non-linear algebraic equations is solved using Newton–Raphson method [8]. Software has been written in C++ using DiffPack numerical library [33].

Our method. Liquid junction potential is obtained as an asymptotic steady-state solution of time-dependent NPP problem for "infinite" heterogeneous rate constants. We use method of lines with new unconditionally consistent space discretization which is one order of approximation higher than used by Brumleve and Buck [5]. The resulting system of non-linear ordinary differential equations (Cauchy problem) was solved using RADAU5 subroutine [9,19] with adaptive time step. The details of the method are presented in the section "Numerical method". The corresponding software has been written in C++ and linked with FORTRAN code for RADAU5 subroutine.

[1] Planck's original deriviation is quite complicated. Morf (in *Anal. Chem.*, 1977, 49(6), pp 810–813) presented a much simpler derivation and without restriction to monovalent ions.

Table 1
Liquid junction potentials for different sample solutions at 298 K. Values calculated according to Henderson, Planck, the evolutional method described by Sokalski and Lewenstam [29], as well as our method.

	Left bulk solution (M)	Right bulk solution – 3.5 M KCl			
		Liquid junction potential (mV)			
		Henderson method	Planck method	Method 1 [29]	This method
KCl	1	0.220	0.220	0.2	0.220
	0.1	0.624	0.624	0.6	0.626
	0.01	1.028	1.028	0.9	1.032
	0.001	1.432	1.432	0.9	1.431
NaCl	1	−1.927	−1.893	−1.9	−1.895
	0.1	0.211	0.204	0.2	0.205
	0.01	0.987	0.962	0.8	0.966
	0.001	1.452	1.423	1.4	1.422
$CaCl_2$	0.5	−3.748		−3.5	−3.547
	0.05	−0.178		0.2	−0.163
	0.005	0.915		0.9	0.850
	0.0005	1.431		1.4	1.350
HCl	1	15.091	16.206	16.2	16.176
	0.1	4.154	4.900	4.9	4.913
	0.01	1.504	1.776	1.5	1.783
	0.001	1.345	1.536	1.0	1.536
NaX	1	6.829	5.839	5.8	5.846
	0.1	1.976	1.633	1.6	1.638
	0.01	1.389	1.187	1.2	1.192
	0.001	1.643	1.454	1.4	1.454

Where X^- is a large anion having low diffusion coefficient – "protein".

Calculated diffusion potential for different solutions and concentrations are compared in Table 1. The diffusion potential was calculated using the following data: one layer, temperature T = 298.16 K, junction thickness d = 200 μm, dielectric permittivity ε=7.08 × 10^{-10} J^{-1} C^2 m^{-1} ($\varepsilon_r = 80$ for H_2O) and diffusion coefficients (in m^2 s^{-1}): $D_{K^+} = 1.98 \times 10^{-9}$, $D_{Na^+} = 1.35 \times 10^{-9}$, $D_{Ca^{2+}} = 7.98 \times 10^{-9}$, $D_{H^+} = 7.98 \times 10^{-9}$, $D_{Cl^-} = 2.01 \times 10^{-9}$, and $D_{X^-} = 10^{-11}$ m^2 s^{-1}. For every ion all the rate constants were equal $\vec{k}_i = k_i = 100\ m \times s^{-1}$, value big enough so that the process is controlled by diffusion. Uniform initial concentration profiles and electric field distribution in the junction were assumed as follows: $c_i(x, 0) = 0$ for $i = 1, \ldots, r$ and $E(x, 0) = 0$ for $x \in [0, d]$.

One can notice that in the KCl/KCl case (Table 1), which is Lingane's type 1 liquid junction, Planck and Henderson equations give the same values. NPP results agree with these values. Furthermore calculated concentration profiles show the linearity – Fig. 3a. For the KCl/HCl case (Lingane's type 3) the calculated results of diffusion potentials are closer to the Planck solution. This results from the fact that for ions having appreciably different diffusion coefficients the resulting steady-state concentration profiles are not linear, and this is contrary to the Henderson assumption – Fig. 3b.

The time-dependent potential response of liquid junction was investigated, using the 10^{-6} M KCl/3.5 MKCl system. The same data as above, but with Heaviside type initial concentration profiles:

$$c_i(x, 0) = \begin{cases} c_{i,L} & \text{for } 0 \leqslant x < \frac{1}{2}d, \\ c_{i,R} & \text{for } \frac{1}{2}d < x \leqslant \frac{1}{2}d. \end{cases} \tag{19}$$

with $c_{i,L} = 10^{-6}$ and $c_{i,R} = 3.5M$ were used for calculations.

Evolution of the electric potential in this case was shown in Fig. 4 in the logarithmic and linear scales. The time-dependent response can be systematically divided into four stages. First the deviation from electroneutrality (Fig. 5a) and the consequent change of the electric field profiles (Fig. 5b) occurs close to the contact of the solutions, until the value of the electric field reaches the

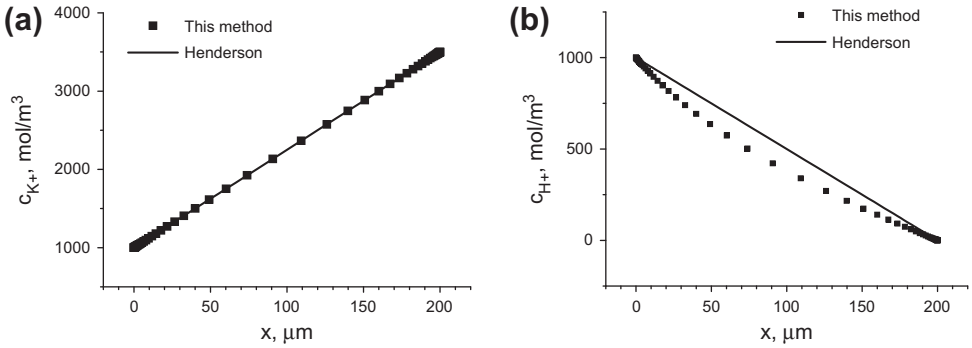

Fig. 3. Liquid junction. (a) Calculated potassium ions concentration profiles for 1 M KCl/3.5 M KCl (left) and (b) protons concentration profiles at steady state for 1 M HCl/3.5 M KCl (right). Calculations using NPP (at steady state) and Henderson models.

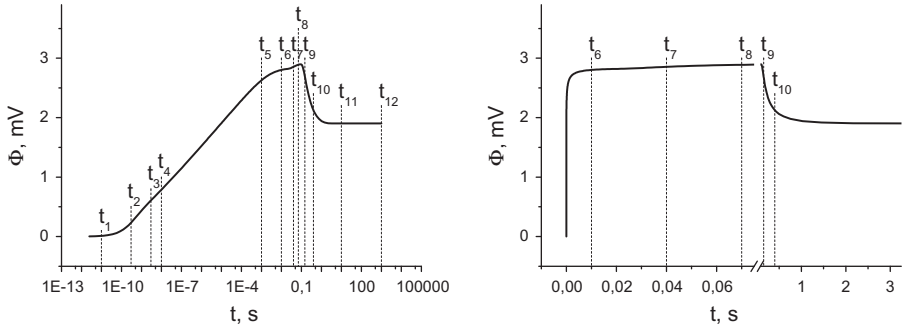

Fig. 4. Liquid junction potential as a function of time in (a) logarithmic and (b) linear scale.

maximum. Secondly the deviation from electroneutrality and consequently the change of the electric field propagate through the system, while their maximum values decrease and the position of maxima moves away from the centre of the junction – Fig. 5b and d. In this stage the potential is convergent to a certain value, as can be clearly seen in Fig. 4b. This value corresponds to the value of the steady state potential in the approach of Dickinson et al. [27], who described the liquid junction in the infinite space (no boundaries). After the deviation from electroneutrality and consenquently the change of electric field reach the boundary (Fig. 5c and d), the third stage begins and the values of maximum deviation from electroneutrality close to the boundary and the electric field at the boundary $E(0,t)$ increases (Fig. 5e and f). When they reach their maximum values, the steady state occurs and the fluxes are constant across the system (in the presented case $J_{K^+}(x,t) = J_{Cl^-}(x,t) = 3.49 \times 10^{-2}\,\mathrm{mol \times m^{-2}\,s^{-1}}$ for $t \geqslant t_{11}$ and $x \in [0,d]$).

The NPP model does not differentiate between the boundary and diffusion potential. In Fig. 6, we present the contribution of these two types of potential to the whole steady-state potential of the membrane in the case of 1 M NaCl/3.5 M KCl. As can be seen, the diffusion potential accounts significantly to the overall potential and cannot be ignored even at the steady state.

3.2. Test of the numerical method in time domain

Binary electrolyte can be useful for testing any numerical method because in this case an *analytical approximate* solution can be derived and compared with numerical one. This case deals with one phase, monovalent binary system, with no external current applied $I(t) = 0$, and equal values of concentrations at the boundaries $c_1(0,t) = c_2(0,t) = c_L, c_1(d,t) = c_2(d,t) = c_R$. In this case, the dimensionless system of the NPP equations is as follows:

$$\begin{cases} \frac{\partial c_1}{\partial t} = D_1 \frac{\partial^2 c_1}{\partial x^2} - D_1 \frac{\partial (c_1 E)}{\partial x}, \\ \frac{\partial c_2}{\partial t} = D_2 \frac{\partial^2 c_2}{\partial x^2} + D_2 \frac{\partial (c_2 E)}{\partial x}, \\ \varepsilon \frac{\partial E}{\partial x} = c_1 - c_2 \text{ for } x \in [0,d], t > 0, \end{cases} \tag{20}$$

with the boundary conditions

$$\begin{cases} c_1(0,t) = c_2(0,t) = c_L, c_1(d,t) = c_2(d,t) = c_R, \\ \left(\varepsilon \frac{\partial E}{\partial t} - D_1 \frac{\partial c_1}{\partial x} + D_2 \frac{\partial c_2}{\partial x} + (D_1 c_1 + D_2 c_2) E\right)_{x=d} = 0. \end{cases} \tag{21}$$

This initial-boundary value problem after inserting $\varepsilon = 0$ results in the system (23)–(26). But, is this procedure meaningful in some way? Yes, because it gives the leading term approximation in the perturbation theory [34] applied to the NPP problem (20) and (21). Namely, it may be proved that for times $t \gg \varepsilon$ the solution can be expressed as an asymptotic expansion

$$c_1(x,t) = \sum_{n=0}^{\infty} c_{1,n}(x,t)\varepsilon^n, \quad c_2(x,t) = \sum_{n=0}^{\infty} c_{2,n}(x,t)\varepsilon^n,$$
$$E(x,t) = \sum_{n=0}^{\infty} E_n(x,t)\varepsilon^n. \tag{22}$$

The substitution of (22) into (20) and (21) yields the sequence of boundary-initial value problems for each order of ε. The term of order ε^0 (which is just the same as the system obtained by inserting $\varepsilon = 0$) reads:

$$\begin{cases} \frac{\partial c}{\partial t} = D_1 \frac{\partial^2 c}{\partial x^2} - D_1 \frac{\partial (cE)}{\partial x}, \\ \frac{\partial c}{\partial t} = D_2 \frac{\partial^2 c}{\partial x^2} + D_2 \frac{\partial (cE)}{\partial x}, \text{ for } x \in [0,d], t > 0, \end{cases} \tag{23}$$

where $c = c_{1,0} = c_{2,0}$ and $E = E_0$. Because dimensionless ε is small (usually on the order of 10^{-8}) we see that the leading term in (22) gives a good approximation to the solution of the original problem (20). The above system may be easily solved as follows.

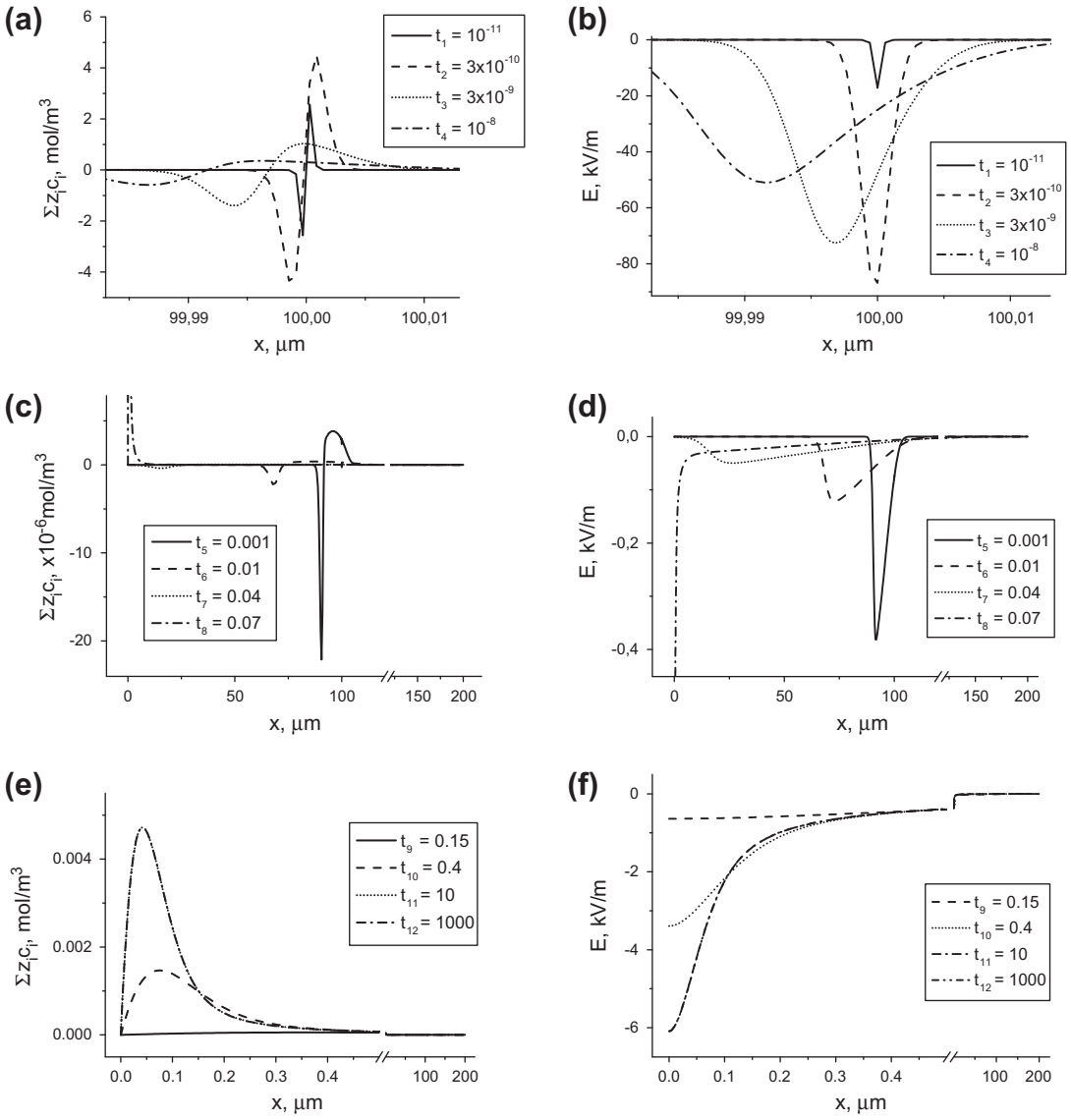

Fig. 5. Deviation from electroneutrality and electric field profiles for 10^{-6}*M*KC1/3.5*M*KC1 liquid junction for various times. Plots for $t_{11} = 10$ and $t_{12} = 1000$ overlaps.

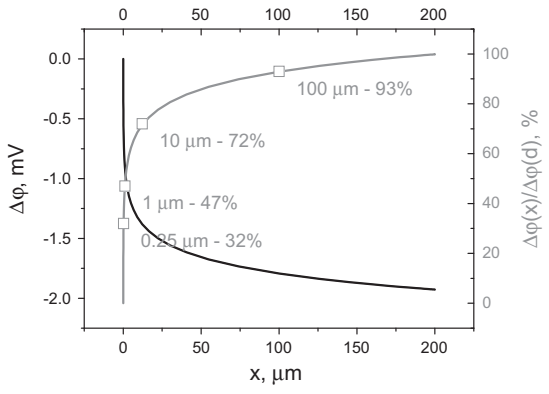

Fig. 6. Liquid junction. Calculated electric potential as a function of $x \in [0, d]$ with its percentage contribution to the overall potential across the junction for the selected values of *x*.

Multiplying the first equation by D_2, second by D_1 and then adding both gives

$$\frac{\partial c}{\partial t} = D\frac{\partial^2 c}{\partial x^2}, \tag{24}$$

where $D = 2D_1D_2/(D_1 + D_2)$. On the other hand if we subtract both equations in (23) we get

$$\frac{\partial}{\partial x}\left(D_1\left(\frac{\partial c}{\partial x} - cE\right) - D_2\left(\frac{\partial c}{\partial x} + cE\right)\right) = 0, \quad \text{for } x \in [0, d], \quad t > 0. \tag{25}$$

Boundary conditions become

$$\begin{cases} c(0,t) = c_L, c(d,t) = c_R, \\ \left((D_2 - D_1)\frac{\partial c}{\partial x} + (D_1 + D_2)cE\right)_{x=d} = 0, \end{cases} \tag{26}$$

and the typical initial condition for liquid junction potential simulation is described with Heaviside type function (19). Eqs. (25) and (26) imply

$$(D_1 - D_2)\frac{\partial c}{\partial x} - (D_1 + D_2)cE = 0,$$

which may be rewritten as

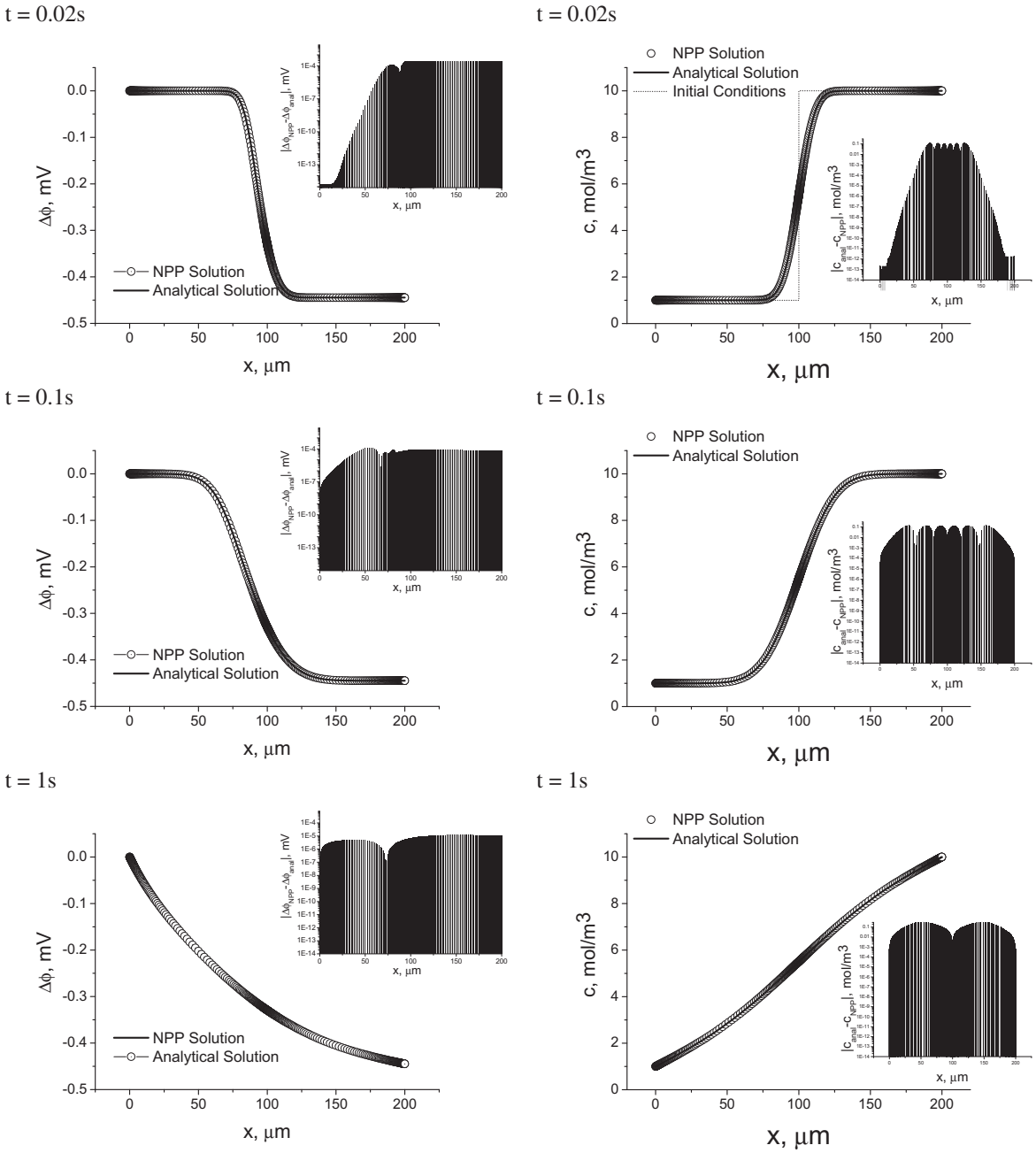

Fig. 7. Liquid junction. Concentration and electric potential profiles calculated at selected times. Comparison of the NPP numerical solution with the analytical one. On the small plots, the absolute difference between analytical and the NPP numerical solution.

$$E(x,t) = \frac{D_1 - D_2}{D_1 + D_2} \frac{\partial \ln c(x,t)}{\partial x}. \tag{27}$$

Using the electrical potential definition $\varphi(\vec{r}) = -\int_0^{\vec{r}} \vec{E} \circ d\vec{\ell}$, where O is some arbitrarily selected reference point, we have

$$\begin{aligned}\Delta\varphi(x,t) &= -\int_0^x E(s,t)ds = -\frac{D_1 - D_2}{D_1 + D_2} \int_0^x \frac{\partial \ln c(s,t)}{\partial s} ds \\ &= -\frac{D_1 - D_2}{D_1 + D_2} \ln \frac{c(x,t)}{c_L}.\end{aligned} \tag{28}$$

Thus, the liquid junction potential across the length of the membrane is given by:

$$\Phi = \Delta\varphi(d) = -\frac{D_1 - D_2}{D_1 + D_2} \ln \frac{c_R}{c_L}. \tag{29}$$

The solution to the problem (24)–(29) may be found in most textbooks [35] and is expressed with the help of the Fourier's series:

$$\begin{aligned}c(x,t) = c_L + (c_R - c_L)\frac{x}{d} + \frac{c_R - c_L}{\pi} \sum_{n=1}^{\infty} \frac{(-1)^n}{n} \\ \times \exp\left(-\left(\frac{2n\pi}{d}\right)^2 Dt\right) \sin\left(\frac{2n\pi x}{d}\right).\end{aligned} \tag{30}$$

Using this concentration profile we can obtain the electric potential by inserting (30) into (28).

Calculations for the system were made using the following data: one phase, temperature $T = 298.16$ K, membrane thickness $d = 200$ μm, dielectric permittivity $\varepsilon = 8.86 \times 10^{-12}$ J^{-1} C^2 m^{-1}

and diffusion coefficients: $D_{K^+} = 1.98 \times 10^{-9}$ and $D_{Cl^-} = 2.01 \times 10^{-9}$ m^2 s^{-1}. For both ions all the rate constants were equal $\vec{k}_i = \overleftarrow{k}_i = 100$ ms^{-1}, value big enough so the process is controlled by diffusion. Heaviside type initial concentration profiles (19), with $c_L = 10^{-3}$ M and $c_R = 10^{-3}$ M were used.

In Fig. 7 we compare the concentration and electric potential profiles at several times obtained from analytical (28) and (30) and numerical (our method) solutions. The agreement is excellent and validates the numerical method.

3.3. The Neumann and Dirichlet boundary conditions

One layer system with the interfaces $\lambda_0 = 0$ and $\lambda_1 = d$ is considered. In this section time evolution of concentrations and electric field are modelled using two different types of boundary conditions: Neumann-like boundary conditions (11) and the Dirichlet boundary conditions (12).

The 0 M KC1/3.5 M KC1 system was chosen to present the influence of boundary conditions. Calculations were performed using the following data: temperature $T = 298 \times 16$ K, junction thickness $d = 200$ μm, dielectric permittivity $\varepsilon = 8.91 \times 10^{-9}$ J^{-1} C^2 m^{-1} and diffusion coefficients: $D_{K^+} = 1.98 \times 10^{-9}$ m^2 s^{-1} $D_{Cl^-} = 2.01 \times 10^{-9}$ m^2 s^{-1}. Heaviside type initial concentration profiles (19), with $c_L = 0$ and $c_R = 3.5$ M were used. Heterogeneous rate constants for the Neumann-like boundary conditions (11) in the range 0.01—100.0 m $\times$ s^{-1} were used in calculations and compared with the results obtained using the Dirichlet boundary conditions.

In Fig. 8, the liquid junction potentials as a function of time for the Neumann-like boundary conditions calculated with different heterogeneous rate constants and for the Dirichlet boundary conditions are compared. The first stages of the potential evolution are independent of the used boundary conditions, as the deviation from electroneutrality and consequent changes of the electric field profile occur far from the boundaries. The larger heterogeneous rate constants the better agreement with results obtained for the Dirichlet boundary conditions is observed. Concentration profiles of the potassium ion in the liquid junction for the time 10 s are presented in Fig. 9a and b. Profiles of the electric field in the junction, calculated for the Neumann-like and Dirichlet boundary conditions for the same time are shown in Fig. 9c. Constant fluxes inside the junction (Fig. 9d), confirm that the steady state is reached. Concentration profiles, electric potential profiles and fluxes, calculated using the Neumann-like boundary conditions for large heterogeneous rate constants ($\geqslant 10$ m $\times$ s^{-1}), also correspond very well to those obtained using the Dirichlet boundary conditions.

All these results confirm, as in the earlier conclusion [6,36], that calculations using the Neumann-like boundary conditions with large heterogeneous rate constants may be substituted by the Dirichlet boundary conditions.

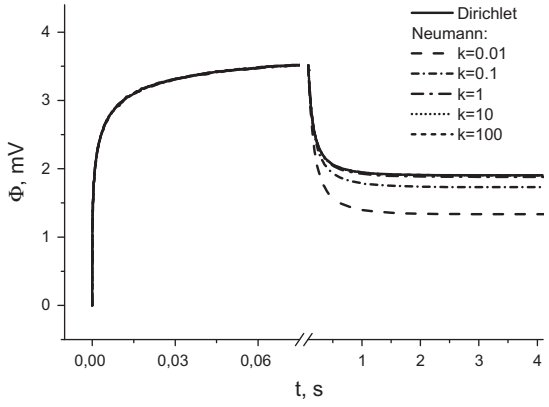

Fig. 8. Comparison of liquid junction potentials as a function of time for the Neumann boundary conditions with different heterogeneous rate constants and for the Dirichlet boundary conditions.

3.4. Bi-ionic case

In this part, the following classical bi-ionic system solution (*MX*)/membrane/solution (*NX*) is considered. Simulations were performed for one layer with the interfaces $\lambda_0 = 0$ and $\lambda_1 = d = 200$ μm, temperature $T = 298.16$ K and dielectric permittivity $\varepsilon = 5.34 \times 10^{-10}$ J^{-1} C^2 m^{-1}. Concentrations of cations in both bathing solutions (MX and NX) were equal $c_{i,L} = c_{i,R} = 10^{-3}$ M.

It is assumed that the membrane is permeable only for cations M^+ and N^+ which can move inside the membrane with the diffusion coefficients $D_{M+} = 10^{-10}$ m^2 s^{-1} and $D_{N+} = 10^{-11}$ m^2 s^{-1}. Membrane is also loaded with anion R^-, which is mobile with diffusion coefficient $D_{R^-} = 10^{-11}$ m^2 s^{-1}. All heterogeneous rate constants for cations are equal $\vec{k}_{M^+} = \overleftarrow{k}_{M^+} = \vec{k}_{N^+} = \overleftarrow{k}_{N^+} = 100$ ms^{-1} and the membrane is not permeable for the anion, that is $\vec{k}_{R^-} = \overleftarrow{k}_{R^-} = 0$.

Calculated concentration profiles of ions M^+, N^+ and R^- for the selected times are presented in Fig. 10. These results are in good agreement with those obtained by Sokalski and Lewenstam [29].

3.5. Ion Selective Electrodes

One of the most important practical applications of the NPP model is the area of ion selective electrodes (ISE). The first ISE, a glass electrode, was invented in 1909 [37]. The first theory for glass electrode potential was developed by Dole [38] and later reformulated by Nikolskii [39]. In the 1960s, both Nikolskii [40,41] and Eisenman [42,43] independently expressed the overall membrane potential as the sum of the *boundary* and *diffusion potentials* under steady state conditions – known today as the Nikolskii–Eisenman (NE) equation [44,45]:

$$\Delta\varphi = \Delta\varphi^0 + \frac{RT}{z_M F} \ln\left(a_M + \sum_N K_{M,N}^{pot} a_N^{z_M/z_N}\right), \tag{31}$$

where subscript M corresponds to main (*primary*) ion and N is an *interfering* one.

This equation in the majority of cases is sufficient for practical analytical chemistry purposes but cannot be used for general theoretical analysis. It is due to the fact that the derivation of the NE equation is based on several assumptions like: (1) the potential at steady state only is considered, thus it does not cover time-dependent cases, (2) the arbitrary split into a boundary and diffusion potential is used, and (3) electroneutrality is assumed.

The electroneutrality condition is often used to simplify the solution of electrodiffusion problems. While in some cases it is justified, there are many others where this assumption is overused. The reason is that this assumption produces a problem, which is much easier to solve. Historically it is understood that such simplification was almost necessary due to lack of high performing computers. But this attitude cannot be defended now, when the access to high computing power is ubiquitous.

Consequently the NE equation is an approximation which fails in many situations [6]. On the other hand modelling may be performed by adopting the NPP equations system, which is general and rich enough in a physical sense to encompass the generation of the membrane potential. The NPP system allows finding the electric potential and concentrations as functions of space and time. These remarks are also valid in the field of ISEs, even though they are generally used in the steady state. Of course the NE equation is derived under the steady state assumption, but its derivation is based on further simplifications. On the other hand the NPP system, integrated up to the time when the steady state is

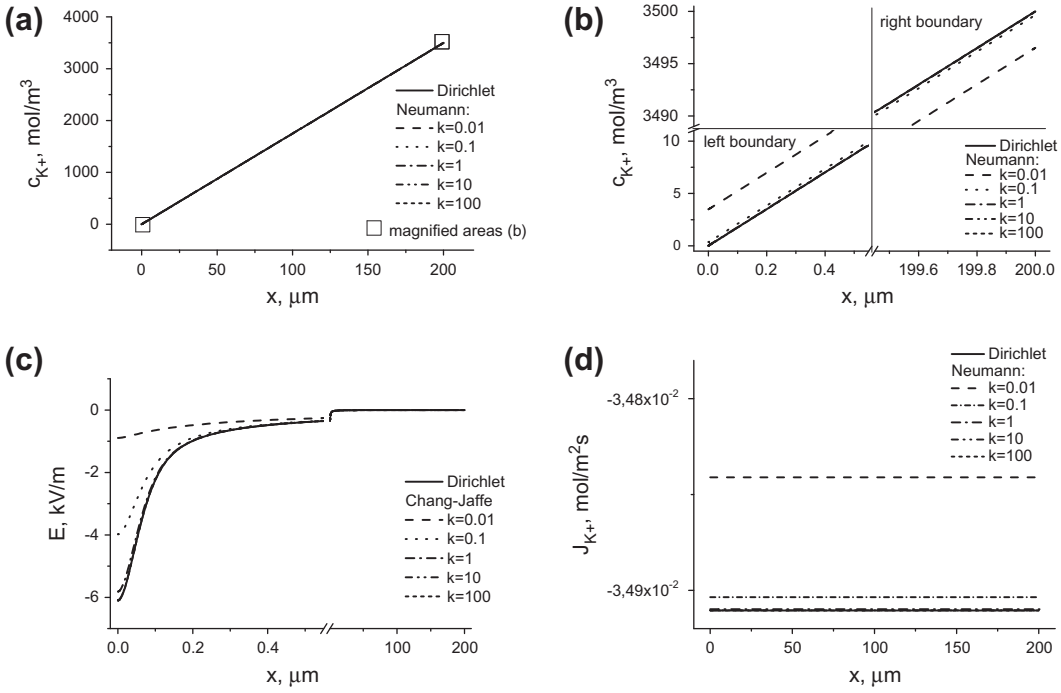

Fig. 9. Concentration of the potassium ion (a) with magnified areas at left and right (b), electric field space profiles (c), and fluxes distribution (d) in the liquid junction at a steady state (for 10 s).

reached, gives better results for the modelling of ISE potential response [46,47].

The first example of the application of the model to ISE is demonstrated in Fig. 11. The calibration curve obtained from one-layer NPP simulation is compared with experimental one [48] showing good agreement. Calculations were carried out using the following data: temperature $T = 298.16$ K, thickness $d = 200$ μm, dielectric permittivity $\varepsilon = 2.12 \times 10^{-10}$ J^{-1} C^2 m^{-1}. Diffusion coefficients in the PCV DOS membrane were defined to be equal as in water: $D_{K^+} 1.98 \times 10^{-9}$ m^2 s^{-1}, $D_{Li^+} = 1.03 \times 10^{-9}$ m^2 s^{-1} and $D_{Cl^-} = 2.01 \times 10^{-9}$ m^2 s^{-1}. The heterogeneous rate constants were (all in $m \times s^{-1}$): $\vec{k}_{K^+} = \overleftarrow{k}_{K^+} = 100$ (at both boundaries), $k^L_{Li^+} = 100$, $\vec{k}^L_{Li^+} = 25$, $k^R_{Li^+} = 100, \vec{k}^R_{Li^+} = 25$, all $k_{Cl^-} = 0$,(superscript R stands for the right and L for the left boundary). The steady state ISE potential was found as an asymptotic value of the time-dependent evolving potential based on NPP model.

In certain cases, processes outside the membrane strongly influence the potential of ISEs. This may result in an overshoot time dependent potentiometric response (first observed by Lindner et al. [49] for solid state ISEs). The fact that this transient-state response is the effect of the presence of the diffusion layer is shown in works of Lindner et al. [50], Lewenstam et al. [51,52] and Bakker et al. [53]. This obviously calls for multi-layer NPP model – Eqs. (1)–(4).

The time-dependent response with the overshoot for ISE was calculated using our method with two layers ($\alpha = 2$) and compared with experimental results of Grätzl and Lindner et al. [50]. Computations were made using the following data: temperature $T = 298.16$ K, layers thicknesses $d_1 = 29$ μm and $d_2 = 100$ μm, dielectric permittivities $\varepsilon_1 = 7.08 \times 10^{-10}$ J^{-1} C^2 m^{-1} and $\varepsilon_2 = 2.12 \times 10^{-10}$ J^{-1} C^2 m^{-1}. Diffusion coefficients in watery diffusion layer were set to: $D^1_{K^+} = 1.98 \times 10^{-9}$ m^2 s^{-1}, $D^1_{Na^+} = 1.34 \times 10^{-9}$ m^2 s^{-1} and $D_{Cl^-} = 2.01 \times 10^{-9}$ m^2 s^{-1}. Diffusion coefficients in the membrane were assumed to be 6 orders of magnitude lower than in water $\left(D^2_i = 10^{-6} \times D^1_i\right)$. Fast ionic transfer between bulk and diffusion layer is considered $\left(\vec{k}_{K^+} = \overleftarrow{k}_{K^+} = \vec{k}_{Na^+} = \overleftarrow{k}_{Na^+} = \vec{k}_{Cl^-} = \overleftarrow{k}_{Cl^-} = 100 \text{ ms}^{-1}\right)$. Membrane is not permeable for the anion: $\vec{k}^2_{Cl^-} = \overleftarrow{k}^2_{Cl^-} = \vec{k}^3_{Cl^-} = \overleftarrow{k}^3_{Cl^-}$. Cations leave the membrane with the heterogeneous rate constants $k^2_{K^+} = \vec{k}^3_{K^+} = k^2_{Na^+} = \vec{k}^3_{Na^+} = 10^{-4}$ ms^{-1} and enter it with the rates: $\vec{k}^2_{K^+} = k^3_{K^+} = 5 \times 10^{-5}$ ms^{-1} and $\vec{k}^2_{Na^+} = k^3_{Na^+} = 8 \times 10^{-7}$ ms^{-1}.

The potential responses as functions of time for the theoretical and the experimental ISE (Fig. 12) show qualitative agreement. The quantitative agreement can be achieved provided that we know real physical and chemical parameters (i.e., diffusion coefficients, rate constants, etc.). This may be obtained by solving the suitable inverse problem for experimentally measured responses. The idea of this approach based on electrochemical impedance spectra has been recently published [54].

The occurrence of the low detection limit of [55] is the effect of the presence of the diffusion layer, therefore calls for a multi-layer approach as well. In [56], a detailed comparison of our method with other models, sufficient for the description of the considered case, was made. The influence of various parameters, such as concentrations in inner solution, layers thicknesses, diffusion coefficients, heterogeneous rate constants and time of measurement was discussed. Finding optimal values of these parameters can have a crucial impact on the design of new electrodes. Inverse problem, estimating these NPP parameters in order to obtain the lowest detection limit was presented in [57].

3.6. Electrochemical Impedance Spectroscopy

Electrochemical impedance spectroscopy (EIS) is a technique for the versatile characterisation of interfacial processes and structures, based on their electrochemical responses. It is a very powerful tool for the analysis of complex electrochemical systems [58]. From the more general perspective it can be viewed as a particular implementation of Fourier transform to *Linear Systems*. Mathematically speaking, such a system can be regarded as a linear operator $L : i \mapsto u$ that exhibits also *time-invariance* property

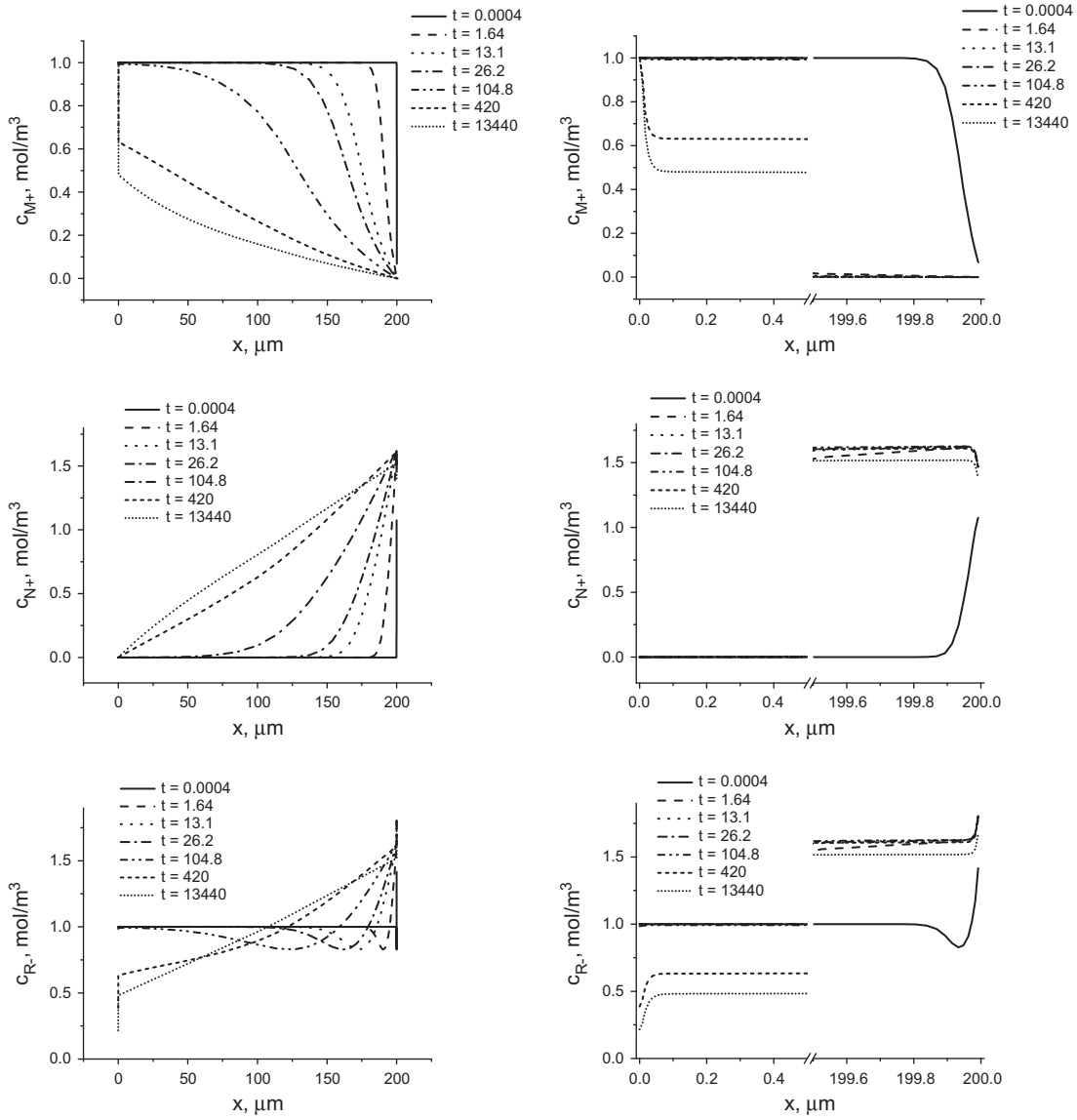

Fig. 10. Bi-ionic case – calculated concentration profiles for ions M^+, N^+ and R^- and for selected times (in seconds).

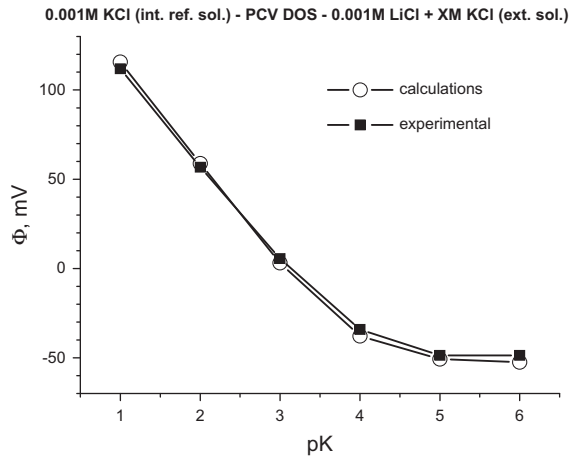

Fig. 11. Calibration curve for PCV DOS ion-selective electrode – comparison of calculated (using the NPP model and described numerical method) and experimental results; Φ – membrane electric potential, $pK = -\log c_{K^+}$.

$L(i(t-\tau)) = u(t-\tau)$. This is a way of saying that parameters of the system are independent of time. The importance of the Fourier transform in the analysis of linear systems is due to the fact that if the input is an exponential periodic $e^{i\omega t}$, then the output is proportional to the input $L(e^{i\omega t}) = H(\omega)e^{i\omega t}$ where $H(\omega)$ is generally a complex number and is called the system (or the transfer) function. In the field of electrochemistry and electrical engineering it is referred to as the *impedance* and denoted by $Z(\omega)$.

Electrochemical impedance is usually measured by applying a time dependent potential to an electrochemical cell and measuring the current through the cell. Conversely, a small current perturbation can be applied and the resulting potential response analyzed. Suppose that we apply a sinusoidal or step current excitation. The response to this current is a time evolving electric potential, containing the excitation frequency and its harmonics. This excitation-response characteristic can be compactly and clearly presented in the graphical form of the so called impedance spectrum on the complex plane $\mathbb{C}$.

EIS is normally performed using a small excitation signal so that the cell's response is linear, making the use of the Fourier transformation possible. In EIS we measure an electrochemical cell's

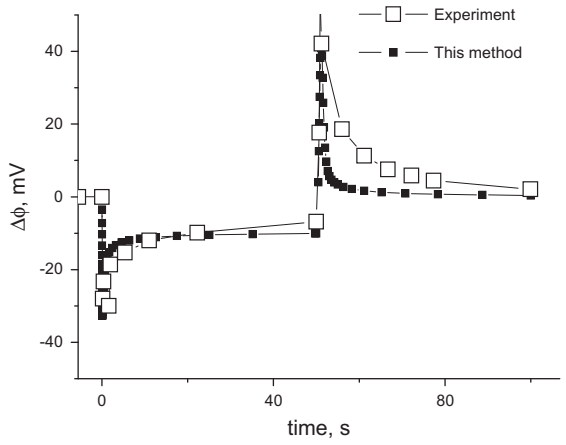

Fig. 12. The overshoot time-dependent response – comparison of calculated (using the NPP model and described numerical method) and experimental results [50].

complex impedance over a wide range of AC frequencies or use the fundamental contribution of the Brumleve and Buck paper [5] by applying only one step-like perturbation to the system. Typically, several cell elements and cell characteristics contribute to the system's impedance spectrum. A partial list of possible elements can include: (1) electrode double layer capacitance, (2) electrode kinetics, (3) diffusion layer and (4) solution resistance.

One commonly used technique in EIS is building an equivalent circuit model which corresponds to the electrochemical system [58]. Such a circuit allows to obtain the EIS spectrum relatively easily. However there are several problems in this approach: (1) the equivalent circuits may not be unique, (2) it is not always possible to describe complex electrochemical behaviour with such circuit elements. In this paper we follow the idea of calculating the EIS spectra put forward by Brumleve and Buck [5]. This approach is more fundamental and universal and it refers directly to the physical processes in the system. Namely, it is based on the NPP model in which the current perturbation is treated as an input parameter and the time-dependent electric potential profile is calculated as an output.

In this section we present the same technical details pertaining to this approach.

3.6.1. Computation of electrochemical cell impedance

If a small current perturbation $I(t)$ is applied to the system, the Fourier transformation of the time response of the electric potential $V(t)$ allows us to obtain the complex impedance. The usual formula for the Fourier transform $f^*(\omega)$ of a function $t \mapsto f(t)$ is $f^*(\omega) = \int_{-\infty}^{\infty} f(t)e^{-i\omega t}dt$, where $i = (0,1) \in \mathbb{C}$ is the imaginary unit.[2] The well-known definitions are as follows:

$$\begin{aligned} Z^*(\omega) &= -V^*(\omega)/I^*(\omega), \\ Z^*(\omega) &= Z'(\omega) + iZ''(\omega), \\ V^*(\omega) &= V'(\omega) + iV''(\omega), \\ I^*(\omega) &= I'(\omega) + iI''(\omega), \end{aligned} \tag{32}$$

where the real part of a complex value is denoted by prime ($'$) and the imaginary part by double prime ($''$). The real and imaginary components of the Fourier transformation of the potential as function of time are given by

$$\begin{aligned} V'(\omega) &= \int_0^{\infty} (V(t) - V_{\infty}) \cos(\omega t)dt, \\ V''(\omega) &= \int_0^{\infty} (V(t) - V_{\infty}) \sin(\omega t)dt + V_{\infty}/\omega, \end{aligned} \tag{33}$$

where $V_{\infty} = \lim_{t\to\infty} V(t)$. Analogous formulae are used to calculate $I'(\omega)$ and $I''(\omega)$.

If the current step of magnitude ΔI is applied, which means the following current profile

$$I(t) = \begin{cases} \Delta I & t > 0, \\ 0 & t \leqslant 0, \end{cases} \tag{34}$$

then the components of the transformation of $I(t)$ are: $I'(\omega) = 0, I''(\omega) = -\Delta I/\omega$ hence the resulting real and imaginary parts of the impedance are given by

$$\begin{aligned} Z'(\omega) &= -V''(\omega) \cdot \omega/\Delta I, \\ Z''(\omega) &= V'(\omega) \cdot \omega/\Delta I. \end{aligned} \tag{35}$$

From the simulations of the time dependant NPP system we obtain the values of $V = V(t)$ at some discrete times $\{t_k\}$ These values may be used to calculate approximately the integrals appearing in the definition of the Fourier transformations (33). There are many possible *quadratures* in numerical textbooks but here we adopt the idea proposed in [4]. Namely, on each interval $[t_k, t_{k+1}]$ the value $V(t)$ is interpolated by a linear function

$$V(t) = \frac{t - t_k}{t_{k+1} - t_k}(V(t_{k+1}) - V(t_k)) + V(t_k) \text{ for } t_k \leqslant t \leqslant t_{k+1}. \tag{36}$$

This approximated potential is inserted into the integrals leading to expressions of the type

$$\begin{aligned} &\int_{t_k}^{t_{k+1}} t\cos(\omega t)dt, \int_{t_k}^{t_{k+1}} t\sin(\omega t)dt, \int_{t_k}^{t_{k+1}} \cos(\omega t)dt, \\ &\int_{t_k}^{t_{k+1}} \sin(\omega t)dt, \end{aligned} \tag{37}$$

which can be easily calculated analytically, that ultimately leads to the following expressions:

$$V'(\omega) = \sum_k \Delta V'_k, V''(\omega) = \sum_k \Delta V''_k + V_{\infty}/\omega, \tag{38}$$

where

$$\begin{aligned} \Delta V'_k = {} & (V(t_{k+1}) - V(t_k))(\cos\omega t_{k+1} - \cos\omega t_k)/\omega^2(t_{k+1} - t_k) \\ & + (V(t_{k+1}) - V_{\infty})\sin\omega t_{k+1} - (V(t_k) - V_{\infty})\sin\omega t_k)/\omega. \end{aligned} \tag{39}$$

$$\begin{aligned} \Delta V''_k = {} & (V(t_{k+1}) - V(t_k))(\sin\omega t_{k+1} - \sin\omega t_k)/\omega^2(t_{k+1} - t_k) \\ & + (V(t_{k+1}) - V_{\infty})\cos\omega t_{k+1} - (V(t_k) - V_{\infty}) \\ & \times \cos\omega t_k)/\omega. \end{aligned} \tag{40}$$

In fact these expressions are nothing more than just applying the composite trapezoidal formula on the interval with grid points $0 = t_0 < t_1 < \cdots < t_{\infty}$, where t_{∞} denotes the time at which the system attains a stationary state. Using these expressions one can calculate $Z'(\omega)$ and $Z''(\omega)$ from Eq. (35) for a range of frequencies ω. Plotting points $(Z'(\omega), Z''(\omega))$ on the complex plane $\mathbb{C}$ for different ω treated as parameter gives the conventional graphical presentation of the complex impedance spectrum.

The above considerations are detailed enough for computer implementation to obtain the impedance spectra based on the NPP model. Suitable computer code using formulae (38)–(40) is a

[2] Different conventions are used for the Fourier integral. Some authors use the formula with factor that is

$$F(\omega) = \frac{1}{\sqrt{2\pi}} \int_{-\infty}^{\infty} f(t)e^{-i\omega t}dt$$

or

$$F(\nu) = \int_{-\infty}^{\infty} f(t)e^{-i2\pi\nu t}dt$$

Basically, all are equivalent except for multiplicative factors appearing in the Fourier integral and the inverse formula.

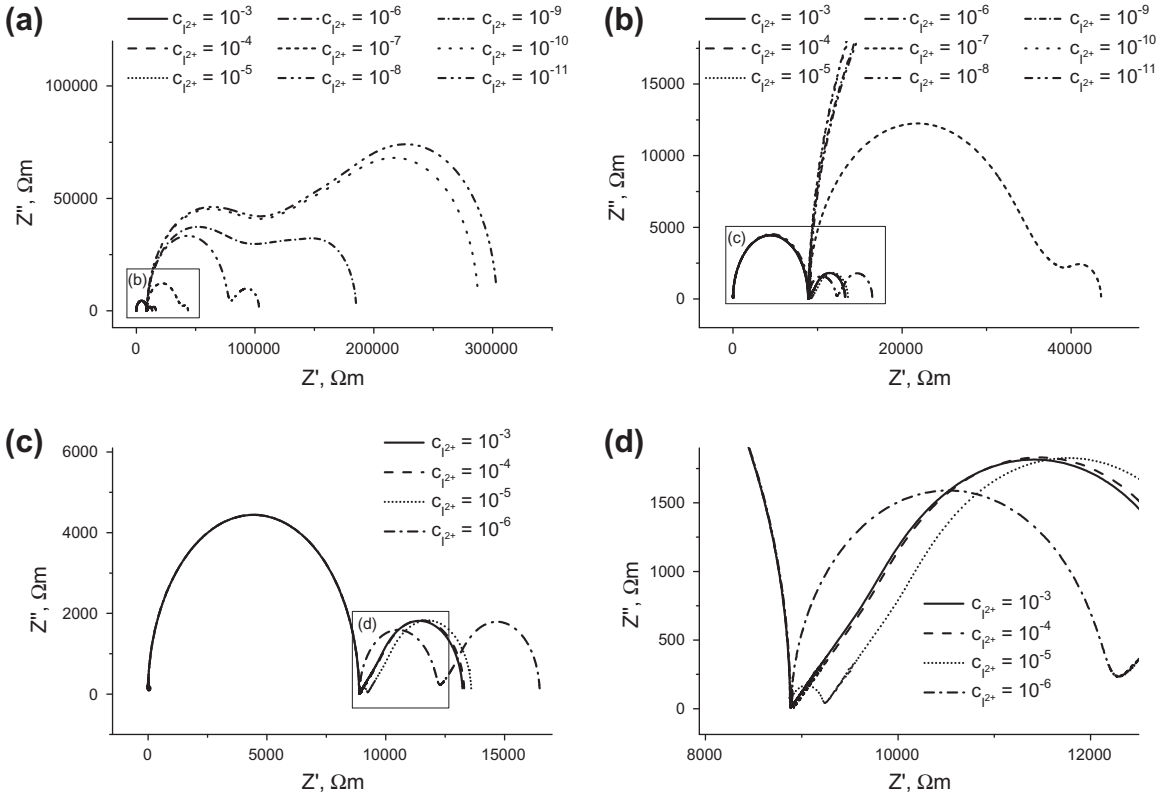

Fig. 13. Complex impedances for ISE, with the concentration of the primary ion in the sample $c_{I^{2+},L}$ varied in the range 10^{-11}–$10^{-3} mol \times m^{-3}$, calculated using our method.

part of the software. Calculations using this method are in good agreement with the results of methods presented in [5,13].

Fig. 13 shows the impedance spectra obtained for ISE, using the presented method for the following data: one layer, temperature $T = 298.16$ K, membrane thickness $d = 200$ μm and dielectric permittivity $\varepsilon = 8.91 \times 10^{-11}$ J^{-1} C^2 m^{-1}. Diffusion coefficients are assumed to be equal: $D_{I^{2+}} = D_{J^+} = D_{X^-} = 10^{-11}$ m^2 s^{-1}. The concentration of the primary ion in the inner solution is $c_{I^{2+},R} = 10^{-2}$ mol × m^{-3} and in the sample varies in the range $c_{I^{2+},L} = 10^{-11}$–10^{-3} mol × m^{-3}. Constant concentrations of the interfering ion in the sample $c_{J^+,L} = 0.15$ mol × m^{-3} and inner solution $c_{J^+,R} = 0$. The membrane is not permeable for the counter ion: $\vec{k}_{Cl^-} = k_{Cl^-} = 0$. For the primary ion, all rate constants were the same $\vec{k}_{I^{2+}} = k_{I^{2+}} = 10^{-4}$ m × s^{-1}. The interfering ion leaves the membrane at the same rate as the primary ion $\overleftarrow{k}_{J^+} = 10^{-4}$ m × s^{-1}, but enters it with a heterogeneous rate constant $\vec{k}_{J^+} = 10^{-10}$ m × s^{-1} which corresponds to the ISE selectivity $K = 10^{-6}$ [56].

The arcs obtained for $c_{I^{2+},L} \geqslant 10^{-3}$ mol × m^{-3}, as well as the ones obtained for $c_{I^{2+},L} \leqslant 10^{-11}$ mol × m^{-3}, overlap. With the change of concentration between these values, the arcs shift from one shape to another (Fig. 13a). This intermediate region of concentrations is the region where the electric potential is the effect of both ions (for $c_{I^{2+},L} \geqslant 10^{-4}$ mol × m^{-3} it depends on the primary ion and for $c_{I^{2+},L} \leqslant 10^{-11}$ mol × m^{-3} on the interfering one), therefore it is non-linear with the change of concentration. This shift in the intermediate region has been already observed, both in theory [13,54] and in the experiment [59].

For high concentrations of primary ion $c_{I^{2+},L} \geqslant 10^{-4}$ mol × m^{-3}, interfacial kinetics is sufficiently fast so only two arcs are predicted [60,61]. For $c_{I^{2+},L} = 10^{-5}$ mol × m^{-3}, the third arc at middle frequencies appears (Fig. 13d). This arc is attributed to the interface impedance [13] and has been already shown, but for the bi-ionic case, in [5,13,54]. With further lowering of the concentration, the interfacial kinetics becomes sufficiently fast, so the intermediate frequency arc grows.

The decrease of concentration of the primary ion $c_{I^{2+},L}$ causes also the low-frequency arc to grow. The middle-frequency arc for low primary ion concentrations grows faster than the low-frequency one for the concentrations in the range $c_{I^{2+},L} = 10^{-8}$–10^{-5} mol × m^{-3} (Fig. 13c and d) and even dominates in the range $c_{I^{2+},L} = 10^{-9}$–10^{-7} mol × m^{-3} (Fig. 13b). Further decrease of the primary ion concentration (i.e. $c_{I^{2+},L} \leqslant 10^{-10}$ mol × m^{-3}) causes the low-frequency arc to start dominating in the plot.

The electrochemical impedance spectra can be used to establish various parameters of the system, such as diffusion coefficients or heterogeneous rate constants. The formulation of the inverse problem, based on our method combined with the Hierarchical Genetic Strategy [62], has been recently published [63].

4. Discussion and conclusions

The numerical procedure based on the method of lines for time-dependent electrodiffusion transport was developed and implemented in C++ language. Two types of boundary conditions were considered, namely, the Neumann boundary conditions for fluxes and standard Dirichlet conditions for concentrations values. The finite difference space discretization with suitably selected weights based on a non-uniform grid was applied. This allowed a higher order of consistency rather than the one put forward by Brumleve and Buck. After using the method of lines the original NPP problem being an initial-boundary value problem for partial differential equations (PDEs) was transformed to the initial (Cauchy) problem for the system of ordinary differential equations (ODEs). The resulting system of ODEs exhibits stiffness behaviour which requires special numerical treatment. It was effectively solved using

the RADAU5 (Radau IIA), RODAS (Rosenbrock) and SEULEX (semi-implicit Euler) ODEs integrators.

The applications to selected electrochemical systems: liquid junction, bi-ionic case and ion selective electrodes were demonstrated. Steady state solutions of the NPP problem for "infinite" heterogeneous rate constants (corresponding to diffusion potential) using our method were compared with the Sokalski-Lewenstam method and the classical Planck and Henderson methods. Good agreement in this case was observed. Some deviations were noticed for the HCl/KCl system between approximate solutions of Planck and Henderson. The solution of the NPP problem, (independent on the chosen method – see Table 1) is closer to the Planck solution. This can be explained by the large difference of diffusion coefficients which leads to non-linear concentration profiles contrary to the assumed linearity of concentration in the Henderson derivation.

In a general case, no analytical solution of the NPP problem is available. But for some special cases it is possible to obtain such a solution. We used such a special case for a transient NPP problem – binary electrolyte with the Dirichlet boundary conditions and initial concentration profiles given by a step-function – for testing the numerical solution. Very good agreement between analytical and numerical (our method) solutions was observed.

Two types of boundary conditions were tested for a liquid junction case. As it was expected [36], the results show that for large heterogeneous rate constants (appearing in the Neumann boundary conditions) solutions of the NPP problem are consistent with the Dirichlet boundary conditions for concentrations (assumed also in the Planck and Henderson models).

This method was also tested for other systems. The first was the textbook example of a bi-ionic case. The obtained results (concentration profiles for different times) showed good agreement with those obtained by Sokalski and Lewenstam [29]. The second were ion selective electrodes which have a great practical importance. Calculations of a calibration curve membrane potential using our method corresponded well to experimental data. Calculated and experimental time-dependent responses of ISE showed the same tendencies, though the exact agreement between our method and the experimental data is not achieved.

The simulations of the NPP model were also used for electrochemical impedance spectroscopy. An effective algorithm for obtaining the impedance spectra [5] was implemented and tested. This gives an alternative freely available tool for EIS analysis other than a commonly used circuit building approach.

The above examples demonstrate some capabilities of the presented numerical method and software that can be effectively used for simulations of electrodiffusion problems. Ubiquitous access to modern personal computers (with high performing processors) make it possible for almost everyone to simulate more advanced electrodiffusion models than commonly used simple formulae, such as Planck, Henderson, Goldman and Nikolskii-Eisenman. Thus, we promote the use of the full form of the Nernst–Planck and Poisson (NPP) problem, that is including explicitly the electric field as an unknown variable with no simplifications like electroneutrality or constant field assumptions. An effective method of a numerical solution of the NPP problem for an arbitrary number of ionic species with different valence numbers either for a steady state or transient state was shown. The presented formulae – the numerical solution to the NPP problem – can be taken up and implemented by anyone. Moreover we make the resulting software freely available to anybody interested in using it.

At this stage the model (and consequently the software) has several limitations. Among them we mention: (1) the dielectric permittivity and diffusion coefficients have no dependence on concentrations, (2) activities are equal concentrations (ideal solutions), (3) no reaction terms and (4) one dimensional geometry. In further developments we are going to address those shortcomings. While the first three constraints can be relatively easy to overcome the last (which means a transition to higher dimensional models) raises a real challenge.

Acknowledgments

This work was supported by the National Centre for Research and Development Grant No. 153217 and by the Polish Ministry of Higher Education and Science – AGH Grant No. 11.11.160.800. Financial support from the Graduate School in Chemical Engineering is gratefully acknowledged.

Appendix A. Space discretization on an uneven grid

The discretization formulae for derivatives on an uneven grid are fairly standard [7]. In general case the formulae for approximation of any derivative by the finite differences on any mesh can be obtained from the Hermit interpolation polynomial [8]. But for simple cases (e.g. three or five points schemes) it is preferable to use directly the Taylor expansion. The formulae for the three-point approximation are included here because they are not very common in the electrochemical literature. We also wanted to underline the differences with the approximation applied in the Brumleve and Buck paper [5]. They used the following finite differences

$$f'(x_k) \approx \frac{f(x_{k+1}) - f(x_{k-1})}{\frac{1}{2}(h_{k-1} + h_k)},$$

while we used the following

$$f'(x_k) \approx \frac{h_{k-1}^2 f(x_{k+1}) + (h_k^2 - h_{k-1}^2) f(x_k) - h_k^2 f(x_{k-1})}{h_{k-1} h_k (h_{k-1} + h_k)}.$$

In addition, to approximate the value of a function at $x \in [a, b]$ by the values of it on the boundaries we used a more accurate expression

$$f(x) \approx \frac{(x-a)f(b) + (b-x)f(a)}{b-a},$$

instead of their approximation

$$f(x) \approx \frac{f(b) + f(a)}{2}.$$

The arrangement of the points on a real line to present discretization formulae are given below.

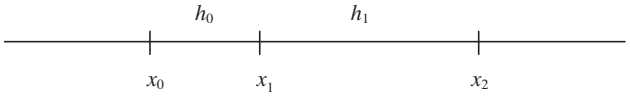

The discretization formulae shown here can be also found in [64,65,7].

A.1. The first derivative

Let $f \in C^3([a, b]; \mathbb{R})$. Then we have

$$f'(x_1) = \frac{h_0^2 f(x_2) + \left(h_1^2 - h_0^2\right) f(x_1) - h_1^2 f(x_0)}{h_0 h_1 (h_0 + h_1)} + r(h_0, h_1),$$

where $r(h_0, h_1) = -\frac{1}{6}(f'''(\xi_0)h_0 + f'''(\xi_1)h_1)\frac{h_0 h_1}{h_0 + h_1}$ for some $\xi_0 \in]x_0, x_1[$, $\xi_1 \in]x_1, x_2[$.

This means that $|r(h_0,h_1)| \leqslant Ch_0h_1$. The constant C is bounded by the maximum of the derivative f''' over the interval $[x_0,x_1]$, i.e. $C \leqslant \frac{1}{6}\max\{|f'''(\xi)| : x_0 \leqslant \xi \leqslant x_1\}$.

In a special case when $h_0 = h_1 = h$, we get the familiar expression

$$f'(x_1) = \frac{f(x_2)-f(x_0)}{2h} + r(h),$$

where $r(h) = -\frac{1}{12}(f'''(\xi_0)+f'''(\xi_1))h^2$ for some $\xi_0 \in]x_0,x_1[$, $\xi_1 \in]x_1,x_2[$.

A.2. The first derivative at the left boundary

We may use the set of points as above, but this time we want to approximate a derivative $f'(x_0)$ at x_0 by the values of f at the points x_1, x_2, which lie to the right of x_0. Using two Taylor expansions at x_0 we can easily calculate

$$f'(x_0) = \frac{-h_1(2h_0+h_1)f(x_0)+(h_0+h_1)^2f(x_1)-h_0^2f(x_2)}{h_0h_1(h_0+h_1)} + r(h_0,h_1),$$

where $r(h_0,h_1) = \frac{1}{6}(f'''(\xi_1)(h_0+h_1) - f'''(\xi_0)h_0)\frac{h_0(h_0+h_1)}{h_1}$ for some $\xi_0 \in]x_0,x_1[, \xi_1 \in]x_0,x_2[$.

This means that the remainder may be bounded as follows: $|r(h_0,h_1)| \leqslant C\frac{h_0}{h_1}(h_0+h_1)^2$.

In a special case, when $h_0 = h_1 = h$, we have

$$f'(x_0) = \frac{-3f(x_0)+4f(x_1)-f(x_2)}{2h} + r(h),$$

where $r(h) = \frac{1}{3}(2f'''(\xi_1) - f'''(\xi_0))h^2$ for some $\xi_0 \in]x_0,x_1[$, $\xi_1 \in]x_1,x_2[$.

Now the reminder is bounded as follows: $|r(h)| \leqslant Ch^2$.

A.3. The first derivative at the right boundary

Now we want to approximate a derivative $f'(x_2)$ at x_2 by the values of f at the points x_0, x_1, which lie to the left of x_2. Using two Taylor expansions at x_2 we can easily derive

$$f'(x_2) = \frac{h_1^2f(x_0)-(h_0+h_1)^2f(x_1)+h_0(h_0+2h_1)f(x_2)}{h_0h_1(h_0+h_1)} + r(h_0,h_1),$$

where $r(h_0,h_1) = \frac{1}{6}(f'''(\xi_0)(h_0+h_1) - f'''(\xi_1)h_1)\frac{h_1}{h_0}(h_0+h_1)$ for some $\xi_0 \in]x_0,x_2[$, $\xi_1 \in]x_1,x_2[$.

Appendix B. Generating of an uneven space grid

The arrangements for the grid points in the membrane are explained here. The grid is exponentially expanding (similar method was used e.g. in [5,66,7]). The case for the denser spacing near the boundaries is explained below. The case for the denser spacing near the centre or both (centre and boundaries) is obtained by simple mirroring.

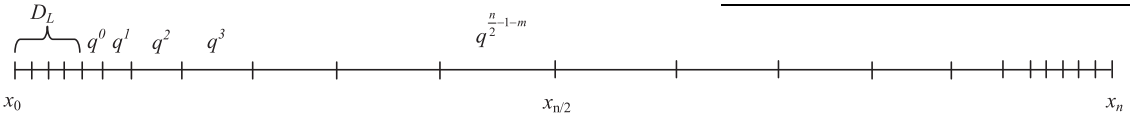

Space grid showing expansion as one moves away from the interfaces. Here q is an expansion factor, so the lengths of the intervals are $D_L \times q^0$, $D_L \times q^1$, …, $D_L \times q^{n/2-1-m}$.

The parameters that are used for generating mesh points are the following: $n+1$ – total number of nodes (including the boundaries), D_L – the Debye length, m – number of equal intervals in the Debye length region, q – the expansion factor of the geometric sequence of the non-uniform intervals.

The expression for q is derived from the equality

$$D_L + \frac{D_L}{m}\left(1+q+q^2+\cdots+q^{\frac{n}{2}-1-m}\right) = \frac{d}{2},$$

where d is the width of the membrane. This gives the equation

$$q^{\frac{n}{2}-m} - 1 = m\left(\frac{d}{2D_L}-1\right)(q-1), \tag{41}$$

which is solved for $q > 1$ numerically (the simple iteration method is sufficient for this purpose although the bisection method was also used to check the results). Eq. (41) has an obvious solution $q = 1$ which of course does not give an expanding sequence. On the other hand it may be easily verified the condition

$$D_L/d < m/n,$$

guarantees the existence of the solution $q > 1$. This condition is readily satisfied in typical simulations because $D_L \sim 10^{-8}, d \sim 10^{-4}$ m, thus $D_L/d \sim 10^{-4}$ and m/n is in the range 10^{-1}–10^{-3}.

References

[1] E. Samson, J. Marchand, Int. J. Numer. Meth. Engin. 46 (1999) 2043–2060.
[2] H. Cohen, J. Cooley, Biophys. J. 5 (1965) 145–162.
[3] H. Chang, E. Jaffé, J. Chem. Phys. 20 (1952) 1071–1077.
[4] A.J. Bard, L.R. Faulkner, Electrochemical Methods: Fundamentals and Applications, second ed., John Wiley & Sons, New York, 2001.
[5] T.R. Brumleve, R.P. Buck, J. Electroanal. Chem. 90 (1978) 1–31.
[6] T. Sokalski, P. Lingenfelter, A. Lewenstam, J. Phys. Chem. B 107 (2003) 2443–2452.
[7] D. Britz, Digital Simulations in Electrochemistry, Springer-Verlag, Berlin Heidelberg, 2005.
[8] A. Quarteroni, R. Sacco, F. Saleri, Numerical Mathematics, Springer-Verlag, New York, 2000.
[9] E. Hairer, G. Wanner, Solving Ordinary Differential Equations II: Stiff and Differential-Algebraic Problems: Stiff and Differential Algebraic Problems, Springer-Verlag, New York, 1996.
[10] J.R. Sandifer, R.P. Buck, Electroanal. Chem. Interface Electrochem. 56 (1974) 385–398.
[11] D.L. Scharfetter, D.L. Gummel, IEEE Trans. Elect. Dev. ED-16 (1969) 64–77.
[12] J.W. Thomas, Numerical Partial Differential Equations: Finite Difference Methods, Springer-Verlag, New York, 1995.
[13] W. Kucza, M. Danielewski, A. Lewenstam, Electrochem. Comm. 8 (2006) 416–420.
[14] W.D. Murphy, J.A. Manzanares, S. Mafé, H. Reiss, J. Phys. Chem. 96 (1992) 9983–9991.
[15] J.W. Perram, P.J. Stiles, Phys. Chem. Chem. Phys. 8 (2006) 4200–4213.
[16] W.E. Schiesser, The Numerical Method of Lines, Academic Press, San Diego, 1991.
[17] R. Filipek, Modelling of diffusion in multi-component systems, in: R. Pampuch, L. Stoch (Eds.), Polish Ceramic Bulletin, The Polish Ceramic Society, Kraków, 2005.
[18] V.M. Volgin, A.D. Davydov, J. Electroanal. Chem. 600 (2007) 171–179.
[19] E. Hairer, G. Wanner, J. Comput. Appl. Math. 111 (1999) 93–111.
[20] W. Gear, IEEE Trans. Circ. Theory 18 (1) (1971) 89–95.
[21] L.K. Bieniasz, J. Electroanal. Chem. 469 (1999) 97–115.
[22] J.W. Thomas, Numerical Partials Differential Equations: Finite Difference Methods, Springer-Verlag, New York, 1995.
[23] L.F. Shampine, Num. Met. Part. Diff. Eqs. 10 (6) (1994) 739–755.
[24] J. Fausek, K. Szyszkiewicz, R. Filipek, Defect Diffus. Forum 323–325 (2012) 81–86.
[25] W.H. Nernst, Z. Phys. Chem. 4 (1889) 165.
[26] M. Planck, Ann. Phys. Chem. 39 (1980) 161–186.
[27] E.J.F. Dickinson, L. Freitag, R.G. Compton, J. Phys. Chem. B 114 (2010) 187–197.
[28] M. Planck, Ann. Phys. Chem. 40 (1980) 561.

[29] T. Sokalski, A. Lewenstam, Electrochem. Comm. 3 (2001) 107–112.
[30] P. Henderson, Z. Phys. Chem. 59 (1907) 118–127.
[31] P. Henderson, Z. Phys. Chem. 63 (1908) 325–345.
[32] J.J. Lingane, Electroanalytical Chemistry, second ed., Wiley, New York, 1998.
[33] H.P. Langtangen, Computational Partial Differential Equations, second ed., Numerical Methods and Diffpack Programming, Springer, 2003.
[34] H.J. Hickman, Chem. Eng. Sci. 25 (3) (1970) 381–398.
[35] J. Crank, Mathematics of Diffusion, Oxfor University Press, 1970.
[36] K. Ludwig, B. Speiser, J. Electroanal. Chem. 608 (2007) 91–101.
[37] W.E. Morf, The Principles of Ion-Selective Electrodes and of Membrane Transport, Akadémiai Kiadó, Budapest, 1981.
[38] M.J. Dole, Am. Chem. Soc. 53 (1931) 4260–4280.
[39] B.P. Nikolskii, Acta Phys. – Chim. USSR 7 (1937) 597–610.
[40] O.K. Stefanova, M.M. Shultz, E.A. Materova, B.P. Nikolskii, Viest. Leningr. Univ. 4 (1963) 93.
[41] M.M. Shultz, O.K. Stefanova, Viest. Leningr. Univ. 6 (1967) 103.
[42] F. Conti, G. Eisenman, Biophys. J. 5 (1965) 247–256.
[43] F. Conti, G. Eisenman, G. Biophys. J. 5 (1965) 511–530.
[44] IUPAC; Pure Appl. Chem. 48 (1976) 129–132.
[45] IUPAC; Pure Appl. Chem. 66 (1994) 2527–2536.
[46] J. Bobacka, A. Ivaska, A. Lewenstam, Chem. Rev. 108 (2008) 329–351.
[47] A. Lewenstam, J Solid State Electrochem. 15 (2011) 15–22.
[48] B. Paczosa-Bator, private communications.
[49] E. Lindner, K. Toth, E. Pungor, Anal. Chem. 54 (1982) 70–72.
[50] M. Gratzl, E. Lindner, E. Pungor, Anal. Chem. 57 (1985) 1506–1511.
[51] A. Lewenstam, A. Hulanicki, T. Sokalski, Anal. Chem. 59 (1987) 1539–1544.
[52] B. Paczosa-Bator, T. Błaż, J. Migdalski, A. Lewenstam, Bioelectrochemistry 71 (2007) 66–74.
[53] E. Bakker, P. Buhlmann, E. Pretsch, Talanta 63 (2004) 3–20.
[54] B. Grysakowski, A. Lewenstam, M. Danielewski, Diffus. Fundam. 8 (2008) 41–47.
[55] T. Sokalski, A. Ceresa, T. Zwickl, E. Pretsch; J. Am. Chem. 119 (1997) 11347–11348.
[56] J.J. Jasielec, T. Sokalski, R. Filipek, A. Lewenstam, Electrochimica Acta 55 (2010) 6836–6848.
[57] J.J. Jasielec, B. Wierzba, B. Grysakowski, T. Sokalski, M. Danielewski, A. Lewenstam, ECS Trans. 33 (26) (2011) 19–29.
[58] E. Barsoukov, J. Ross Macdonald, Impedance Spectroscopy: Theory, Experiment, and Applications, second ed., Wiley-Interscience, 2005.
[59] D. Calvo, J. Bartroli, M. del Valle, Electrochim. Acta 51 (2006) 1569.
[60] C. Gabrielli, P. Hemery, P. Letellier, M. Masure, H. Perrot, M.-I. Rahmi, M. Turmine, J. Electroanal. Chem. 570 (2004) 275.
[61] T.M. Nahir, R.P. Buck, Electrochim. Acta 570 (1993) 2691.
[62] J. Kołodziej, R. Gwizdała, J. Wojtusiak, Hierarchical Genetic Strategy as a Method of Improving Search Efficiency, in: Advances in Multi-Agent Systems, Jagiellonian University Press, 2001, pp. 149–161.
[63] B. Grysakowski, J.J. Jasielec, B. Wierzba, T. Sokalski, M. Danielewski, A. Lewenstam, J. Electroanal. Chem. 662 (2011) 143–149.
[64] D.J. Gavaghan, J. Electroanal. Chem. 456 (1998) 1–12.
[65] M. Rudolph, J. Electroanal. Chem. 529 (2002) 97–108.
[66] S.W. Feldberg, J. Electroanal. Chem. 127 (1981) 1–10.